FLORIDA STATE UNIVERSITY

COLLEGE OF ARTS AND SCIENCES

SEARCH FOR HIGGS BOSON DECAYS TO LEPTOPHILIC LONG-LIVED SCALAR

PARTICLES WITH REGIONS OF INTEREST (ROIS) AND MACHINE LEARNING IN CMS

By

SUHO KIM

A Dissertation submitted to the
Department of Physics
in partial fulfillment of the
requirements for the degree of
Doctor of Philosophy

2022

Suho Kim defended this dissertation on Nov 18, 2022.

The members of the supervisory committee were:

Ted Kolberg

Professor Directing Disseration

Elizabeth Hammock

University Representative

Todd Adams

Committee Member

Kohsaku Tobioka

Committee Member

Peter Hoeflich

Committee Member

The Graduate School has verified and approved the above-named committee members, and certifies that the dissertation has been approved in accordance with university requirements.

To my parents, who always suspected I'd end up here

ACKNOWLEDGMENTS

Thanks to many people.

TABLE OF CONTENTS

LIST OF TABLES

LIST OF FIGURES

ABSTRACT

We present a search for long-lived particles (LLPs) produced in gluon fusion Higgs production mode (ggH), using a novel strategy of Regions of Interest (ROIs). Regions of Interest are collections of pair-wise track vertices fitted by the vertex fitter in CMSSW. The analysis focuses LLPs with lifetimes that result in decays in the tracker region, with concentration on the ggH production mode for the highest Higgs cross-section. Variables of the constructed ROIs become inputs for our Deep Neural Network (DNN) Machine Learning (ML) algorithms, as a main discriminator between the signal and the background. We focus on the Standard Model (SM) τ lepton final state. This final state is particulary interesting, given τ lepton final state exclusion limits are mostly omitted in precedent analyses, due to τ leptons' non trivial reconstruction mechanisms in CMS. In order to trigger on the ggH production mode of the Higgs particle, decaying into its leptonic signature via exotic long-lived scalar particles, we exploit the B-parking trigger. B-parking trigger is newly installed High Level Trigger path in the CMS detector, targetting soft displaced muon. The trigger was installed in 2018, totalling in integrated Luminosity value of $41\mathrm{fb}^{-1}$. No excess of events over the standard model expectation is observed. The results are interpreted in the context of exotic Higgs decays to a pair of long-lived scalars (S). We set limits on the branching ratio of the Higgs to LLPs, $\mathbf{B}(\mathrm{H}\to SS \to \tau\tau\tau\tau)$, as a function of the proper lifetime. The analysis has strongest discriminant power for the scalar particle's lifetime from 1mm to 10mm for 7and 15GeV, and from 10mm to 100mm for 40 and 55GeV. The analysis' exclusion limit on the branching ratio for τ lepton final state ($\mathbf{B}(\mathrm{H}\to SS \to \tau\tau\tau\tau)$) is one of the most stringent results from the LHC detectors. The 9% at 10mm for 7GeV, 5% at 10mm for 15 GeV, 9% at 100mm for 40 GeV, and 20% at 1000mm for 55 GeV are respective values.

CHAPTER 1

INTRODUCTION

The discovery of particles at the electroweak scale, such as the top quark at Fermilab's CDF and D0 [1, 2] and the Higgs boson at the Large Hadron Collider (LHC) in CERN [3, 4], led to discovery of all constituents in the Standard Model (SM). The SM describes the nature of fundamental particles and their interactions with precision. In spite of its success, the SM suffers from the few obstacles: the evidence of neutrino masses and mixing [5], the obsevations of bullet clusters confirming the presence of dark matter (DM) [6, 7, 8, 9, 10], and baryon-antibaryon asymmetry [11] all remain unexplained in the framework of SM. In addition, the SM suffers from the naturalness problem. To solve such issues, one needs to look for physics Beyond the Standard Model (BSM).

To search for the BSM, the high energy physics (HEP) community has completed many researches both in theoretical and experimental sides. Theoretical high energy physics community approached the issue with 2 main approaches. The first approach tackles the issue of precision. Although the SM is very well constrained model, further precision of particles in the SM, especially those in the electroweak scale, gives new insight for the BSM physics. For instance, the CDF collaboration recently discovered a 7σ deviation of the W boson mass from the SM prediction [12]. The W boson mass deviation has been interpreted for new physics using the framework of the Standard Model Effective Field Theory (SMEFT) [13]. In SMEFT, the SM operators from the SM Lagrangian are used to build 5,6,8-dimensional new terms for the Lagrangian. The SMEFT scalar, fermion, or vector extension gives hint for new insight for the BSM and its phenomenology [13]. The other approach aims to build an entirely new Lagrangian term, which can be appended to the current SM Lagrangian term. The BSM Lagrangian introduces new particle fields and should address unsolved issues in the current SM framework. The new particles' mass scale can range from those in the collider level upto the astrophysical level.

To find the new BSM particles, the experimental high energy physics community conducted many different researches based on both collider and astrophysical data. Experimental physicists invested strenuous effort on data from the collider physics, since lightest particles from popular theory, such as supersymmetry (SUSY), were within the collider's hard scattering energy level. Experimentalists searching for the BSM particles can also divide their main approaches into 2, the

first with prompt decay of the BSM particle and the second with long-lived lifetime signature. CMS analysis targeting the BSM particles with prompt lifetime have been fully studied and resulted in no deviation from the SM prediction [14]. However, the second approach, which has not been fully investigated, is when particles decay with Long-Lived signature, in other words, Long-Lived particles (LLP). This signature is uniquely interesting and challenging for scientists. It requires different analysis strategy depending on the mass scale (MS) and lifetime ($c\tau$) of the BSM particle. Thus, this frontier has been perceived as the blue ocean for HEP experimentalists, to the extent that a new detector solely targeting LLPs is planned to be built [15].

In this dissertation, we focus on the LLPs originating from the LHC, specifically the CMS, review precedent analyses, and propose a novel strategy. Searches for LLPs decaying into final states containing jets were investigated at the Tevatron ($\sqrt{s} = 1.96$ TeV) by both CDF [16] and D0 [17] Collaborations, at the LHC by the ATLAS and LHCb Collaborations at $\sqrt{s} = 7$ TeV [18, 19], by the ATLAS, CMS and LHCb Collaborations at $\sqrt{s} = 8$ TeV [20, 21, 22, 23, 24, 25, 26]. More recently, by the CMS [27, 28, 29, 30, 31, 32] and ATLAS Collaborations [33, 34, 35, 36, 37, 38, 39, 40, 41, 42, 43, 44] at $\sqrt{s} = 13$ TeV.

CMS Collaboration released a new result in 2021. In the new paper, the Higgs decaying into LLPs, is created in association with a Z vector boson [45]. This analysis' feynman diagram is displayed in figure 1.1. The new analysis shed light on LLPs with lighter masses thanks to the clean dilepton trigger from the associated Z vector boson. Although exclusion limit on branching ratio of the Higgs to the LLPs to b and d-quark were set below unitarity for analyses above, exclusion limit for τ final state has been omitted or presented with values above 1.

However, the Leptophilic model for Twin Higgs and other Higgs models are also highly motivated [46]. Continuous neglect of τ final state limit is not only a poor practice, but overlooks an important unexplored phase space. This analysis searches for LLPs, originating from the Higgs Portal model with the Higgs' Leptophilic nature. Since the coupling strength of the Higgs' to SM fermions are quantified by the Yukawa couplings, focus on Leptophilic Higgs translates into focuses on τ final state decaying back from the LLPs via the Higgs Portal. The 55 GeV maximum scalar mass is set to investigate only on-shell neutral scalar particles from the Higgs. A minimum 7 GeV mass for scalar particles is required to create on-shell τ-lepton pairs. Feynman diagram of the scalar particle production mechanism is depicted in Figure 1.2. Main challenge and reason for omission of a τ lepton analysis is on the different decay modes of τ leptons. τ leptons decay hadronically and leptonically, with several different sub-decay modes. Its decay mode pie chart and CMS detection

Figure 1.1: Feynman diagram of ZH signal process studied in the most recent CMS analysis paper (2021)
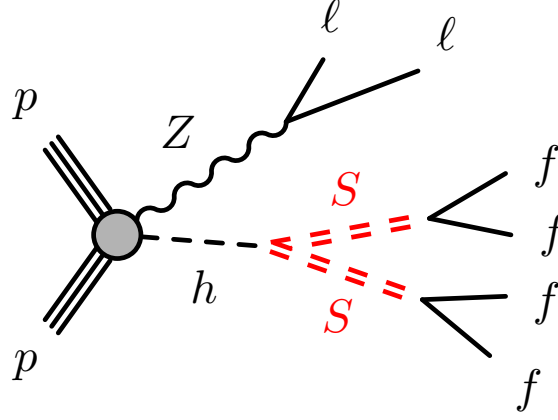
category pie chart are displayed in figures of 1.3 and 1.4 respectively. Developing analysis strategies to optimize the search for each sub-decay modes is extremely complicated, a main reason for the omission or no good exclusion limit in precedent LHC results. To be inclusive of all τ leptons' decay modes, a displaced vertex search can be more efficient than a displaced objects (jet, muon, electrons) search. We exploit the newly developed Regions of Interest mechanism in the tracker volume. Regions of Interest (ROI) form displaced vertex candidates, by fittng pair-wise tracks of Lost-tracks and PackedPFCandidates classes in MINIAOD data into a vertex. ROIs save all relevant track and fitted vertex qualities along with isolation information. These variables are used as input for Machine Learning (ML) algorithms, enabling a highly generic and data-scientific search method.

Figure 1.2: The analysis' signal process feynman diagram. The Higgs is created in gg production mode. The LLP scalar decays into τ lepton.
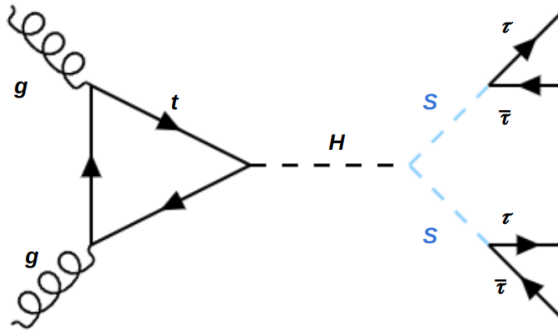
Figure 1.3: τ lepton's decay mode pie chart

Tau lepton decay mode
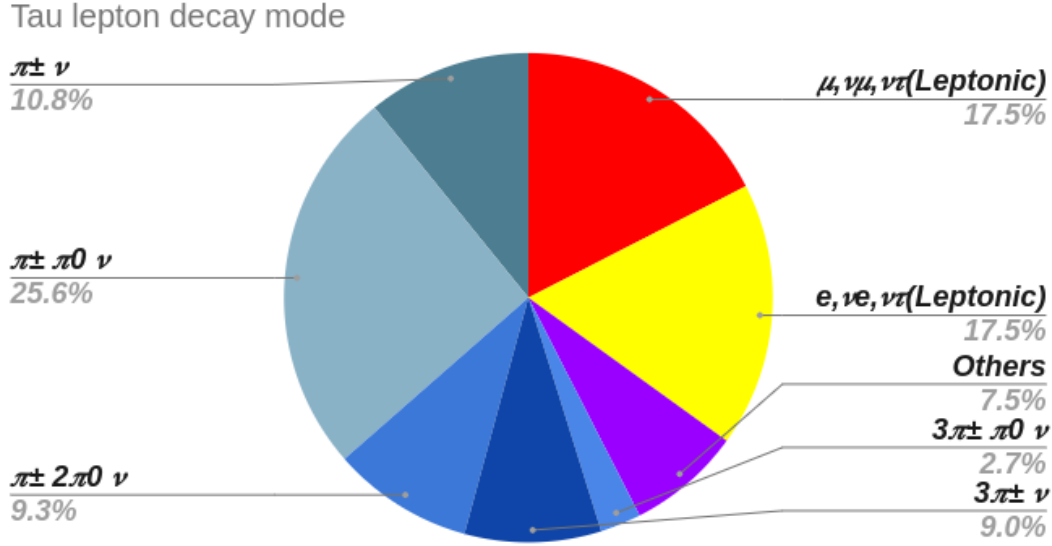
Figure 1.4: τ lepton's detection mode pie chart. Prong means a charged track reconstructed in the tracker volume of the CMS. It corresponds to $\pi^{\pm}$

Tau lepton detection mode

Another challenge is that CMS searches are not optimal for detecting Higgs boson decays due to the soft p_T nature of its decays products. Higgs produced in association with Z vector boson analysis [45] overcame this barrier with help of dilepton trigger. Although ggH production mode gives the largest Higgs crosssection, it complicates the trigger strategy even further. This analysis exploits the τ lepton's leptonic decay, in which the τ lepton decays into a soft muon, using a trigger of B Parking High Level Trigger (HLT) Path implemented in CMS for the 2018 portion of Run 2.

4

The rest of the dissertation is organized as follows. In Section 2, we discuss the theoretical background of the BSM and LLPs in more details. In Section 3, the CMS detector is thoroughly discussed with emphasis on the tracks and the calorimeter, which are relevant detector parts for the analysis. We discuss how the analysis exploited the b-parking trigger in Section 4, with description of its original motive for the trigger's installation. The physics objects and formation of Regions of Interest are described in Section 5. The machine learning algorithms are futher explained in Section 6. The event selections are presented in Section 7. Section 8 describes the data driven background estimation method. Section 9 describes the background estimation method's validation process and systematic uncertainties. Finally, Section 10 presents the results of the search. We conclude with Section 11.

CHAPTER 2

THE STANDARD MODEL AND ITS FUTURE

In Section 1, we introduced the few obstacles facing the SM: Existance of darkmatter, baryon-antibaryon asymmetry, and the evidence of neutrino masses and mixing. The SM Lagrangian, writted as in formula 2.1, does not have particles' fields which can explain those phenomena.

$$\mathcal{L}_{SM} = \mathcal{L}_{Higgs} + \mathcal{L}_{Gauge} + \mathcal{L}_{Kinetic} + \mathcal{L}_{Yukawa} \tag{2.1}$$

Since it can not be explained by any of the particles' fields in the SM, it requires addition of new particles' fields or new terms in the current SM Lagrangian expression. New terms in the SM Lagrangian entails in new vertices in the Feynman diagram, which open the door for a new understanding of the high energy physics. However, if those observations did not exist, the SM is all complete within its own framework only except for the naturalness problem.

The naturalness problem originates from the fact that the SM Higgs is a scalar particle. The formula 2.1 has three different kinds of fields: boson, fermion, and scalar. Quantum Field Theory (QFT), the humanity's mathematical framework used for the SM, explains matter as an excited state of fermion fields, derived from the canonical quantization of the SM Lagrangian's fermion fields. The fermions' fields have chrial symmetry as demostrated in the kinetic term of the SM Lagrangian in formula 2.2 and 2.3.

$$\mathcal{L}_{L_{kin}} = \bar{L} * i\gamma^{\mu} D_{\mu} L + h.c. \tag{2.2}$$

$$\mathcal{L}_{R_{kin}} = \bar{u} * i\gamma^{\mu} D_{\mu} u + \bar{d} * i\gamma^{\mu} D_{\mu} d + h.c. \tag{2.3}$$

, where dirac matrices are summed up over Lorentz indices for Lorentz invariance, lefthand fermion is a doublet for weak force interaction, and right-hand fermion is a singlet separated by the uptype fermion (neutrinos for leptons) and downtype fermion (electrically charged leptons for leptons). Since fermions with left-hand chriality behaves in a different manner from fermions with right-hand chirality, the covariant derivatives are also different for left-hand kinetic term and right-hand

kinetic terms, being defined in 2.4 and in 2.5.

$$D_\mu = i\partial_\mu - \frac{1}{2}g\tau * W_\mu - \frac{1}{2}g'YB_\mu \qquad (2.4)$$

$$D_\mu = i\partial_\mu - \frac{1}{2}g'YB_\mu \qquad (2.5)$$

, where τ is isospin for SU(2) weak force, and g,W are couplings and fields for the weak theory. g' and B are respective variables for quantum electrodynamics (QED). In equations above, we can see the fermions with lefthand chirality are separated from the righthand chirality.

Likewise, the bosons' fields also satify special symmetries in the QFT framework. The boson satisfy the U(1), SU(2) or SU(3) gauge symmetry, and are expressed in gauge terms as in formula 2.6.

$$\mathcal{L}_{Gauge} = -\frac{1}{4}B_{\mu\nu} * B^{\mu\nu} - \frac{1}{4}W_{\mu\nu}^\tau * W_\tau^{\mu\nu} - \frac{1}{4}G_{\mu\nu}^\alpha * G_\alpha^{\mu\nu}. \qquad (2.6)$$

,where B,W,G are QED, weak, quantum chromodynamics (QCD) fields, τ, α are SU(2),SU(3) group indices respectively.

These symmetries provice 1 major advantage in QFT, the renormalization. QFT understands the observed mass of particles in terms of its bare mass and correction as in 2.7.

$$m_f^2 = m_{f,0}^2 + \delta m_f^2. \qquad (2.7)$$

The chrial and gauge symmetries make correction to be zero, and protect fermion and boson fields from the radiative correction in the renormalization process.

Unlike fermions or gauge bosons, the scalar field of the Higgs boson is not protected by any symmetry and is subject to large radiative corrections, especially from the top quark loop. Thus, for the SM to be valid up to the Planck or Grand Unification Theory (GUT) scales of 10^{16} GeV, the necessary radiative corrections are enormous. One needs an exorbitant amount of fine-tuning to fit the Higgs mass at the observed value of 125GeV. One of the most popular solutions to this problem is Supersymmetry (SUSY), which assigns chirality to the Higgs particle. SUSY solves the fine-tuning problem, neutrino masses, and provides a candidate for DM.

Unfortunately, the LHC has found no significant excess over the SM background in their search for SUSY[14]. Although the non-observation of supersymmetric partner particles does not invalidate SUSY, it makes less attractive among the particle physics community. Non-observation of superpartners, particularly the stop (scalar partner of the top quark) has pushed its mass beyond

1TeV. This generates "little hierarchy" problem, but an alternative solution of "neutral naturalness" remains.

In the framework of neutral naturalness, the top partners are not charged under the SM color group. Because of being colorless, their production crosssection is much smaller, and the present limits on the top partner particles are well below 1TeV. Examples of neutral naturalness models are the Twin Higgs [47], Folded SUSY [48], and the Quirky Little Higgs [49] models. Theoretical models provide the possibility of neutral Long-Lived Particles (LLPs), which may be produced in the proton-proton collisions of the LHC, and decay back to SM particles far from the interaction point (IP).[50] If the mirror QCD gluons form scalar glueballs, the SM Higgs boson can become a "Higgs Portal" between the SM and BSM mirror QCD scalar glueballs. In the Mirror SM and Twin SM models, only the SM Higgs boson can interact with both SM QCD and mirror QCD particles as in figure 2.1. BSM mirror QCD scalar glueballs can only decay back to SM particles via Higgs

Figure 2.1: A cartoon display of Higgs Portal process
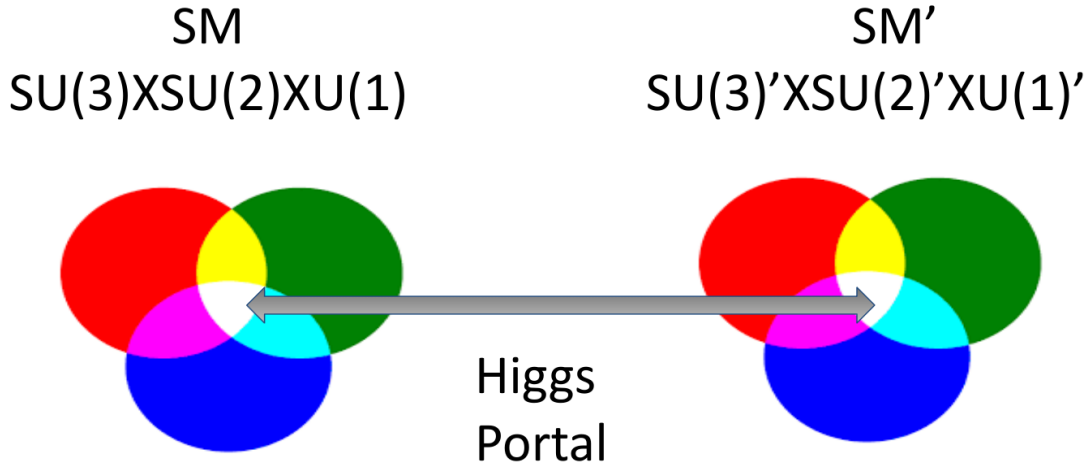
boson decay as well.

Because of its decay as an offshell Higgs boson, its crosssection is highly suppressed. Decay branching ratio to highest mass fermions will be highest following the Yukawa couplings. Decay ratio into b quarks or τ leptons are highest depending on the mirror scalar's mass. However, if the Higgs has leptophilic behavior, decay ratio into τ leptons are always the highest. The displaced decays of the scalars would lead to exotic signatures in the CMS, such as distant innermost tracker hit, displaced vertices, and displaced jets. Phenomenology of long-lived particles in LHC entailed

increase in interest of neutral naturalness framework among the particle physics community. [51, 52]. The long-lived scalar model is shown in the Figure 2.2.

Figure 2.2: A diagram display of Higgs Portal process
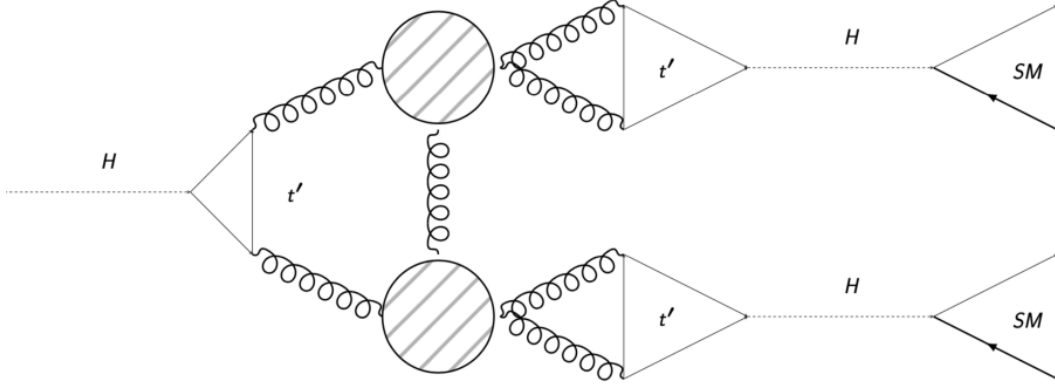
CHAPTER 3

THE CMS DETECTOR

CHAPTER 4

TRIGGER STRATEGY

The analysis' signal process contains SM τ leptons in its final state. In order to exploit the leptonic decay of τ lepton, specifically with muon final state for clean signal, the B-Parking triggers are used. CMS implemented the B-Parking trigger since the year of 2018 of Run 2 for research on lepton universalities. For research of $R(K^*,D^*)$, muonic final state of B mesons are desired. B trigger requires a soft muon with modest displacement (measured using impact parameter) from the primary vertex, exploiting the b quark's long lifetime. B Parking trigger requires a muon with transverse momentum (pT) of 7-12 GeV with impact parameter (IP) 3-6. pp collisions in LHC produce extremely enormous amount of events, which could trigger the B parking trigger paths. Current CPU capacity of CMS is limited and not capable of reconstructing the entire event at such high trigger rate in HLT level. Thus, CMS scouts events, meaning it writes events that passed L1 trigger to a temporary dataset. Later, full HLT and RECO steps are implemented and served as a B-Parking dataset. The prescale factor for BPH triggers is 5-6.

4.1   Global Tags

Table 4.1: Data and MC Global tags used 2018

Data 2018	106X_dataRun2_v29
MC 2018	106X_upgrade2018_realistic_v11_L1v1

4.2   Trigger Paths

We utilize the B-Parking triggers collecting data for the year of 2018. The exact names of paths for B-Parking triggers are listed in Table 4.2. We observe that the trigger efficeincy reaches a plateau after requiring a muon with pT value above that utilizes in the L1 seed.

Below is the trigger efficiency of various BPH trigger paths for different mass and lifetime points of the signal (HToSSTo4Tau) sample

Table 4.2: HLT trigger paths used in the analysis 2018.

Data sample	Trigger
ParkingBPH*-Run2018A	HLT_Mu9_IP6_part*
ParkingBPH*-Run2018B	HLT_Mu12_IP6_part*
ParkingBPH*-Run2018C	HLT_Mu12_IP6_part*
ParkingBPH*-Run2018D	HLT_Mu12_IP6_part*

Figure 4.1: asd
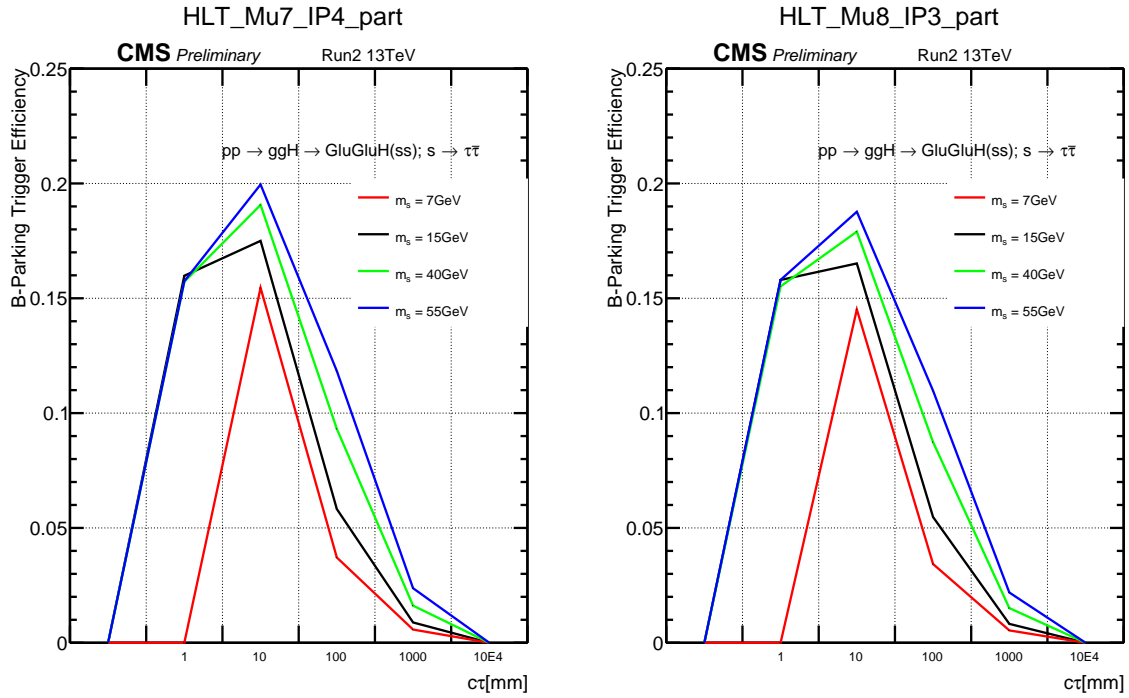
Figure 4.2: eeee
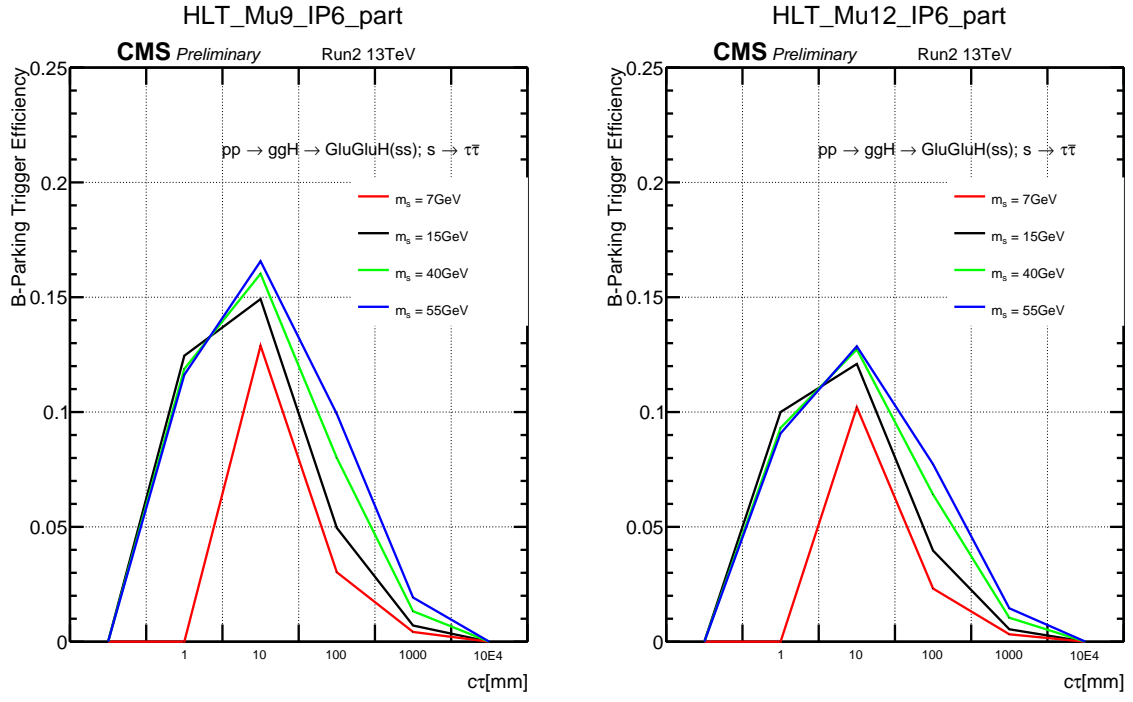
CHAPTER 5

PHYSICS OBJECT DEFINITIONS

In this section, we provide the definitions of physics objects used in the analysis.

5.1   Muons

The analysis sources the SlimmedMuons collection from the MINIAOD MC datasets to produce `selectedPatMuons`. Muon objects are required to have

- $pt \geq 12$ GeV to reach BPH trigger plateau

- $|eta| \leq 1.5$ for L1 seed $|eta|$ cut in BPH trigger

- Pass the Loose ID criterion (isLooseMuon) as described in the Muon POG [53].

Figure 5.1: Data/MC of muon objects
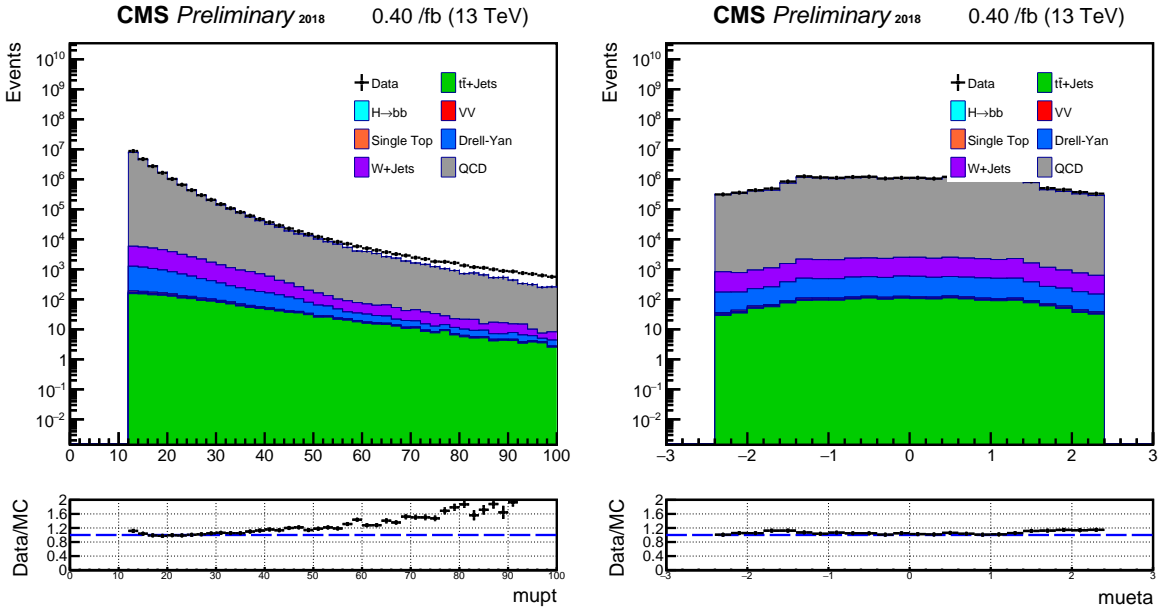
The motivations for isolation requirements on muons are discussed in Section 7.

14

5.2   Jets

The analysis sources SlimmedJets collection from MINIAOD dataset to produce `selectedJets`. CMS reconstructs jets from calorimeter energy deposits using the anti-k_T clustering algorithm with a distance parameter of $R = 0.4$ [54]. Then, the calojets are inputed into the Particle-Flow (PF) algorithms to produce the PFJets collection. Variables in PFJets class are then slimmed to be saved into MINIAOD files. The analysis uses these SlimmedJets for the jets' b tagging scores as well. Jet objects require

- pt $\geq$ 20 GeV

- $|\eta| \leq 2.4$

- $0 \leq$ emEnergyFraction ≤ 0.9

- $0 \leq$ energyFractionHadronic ≤ 0.9

- No selected electron or muon within $\Delta R = 0.4$

The energy fraction cuts above are taken from the recommended Run2 Tight jet ID cuts for particle flow jets [55].

Figure 5.2: Data/MC of jet objects
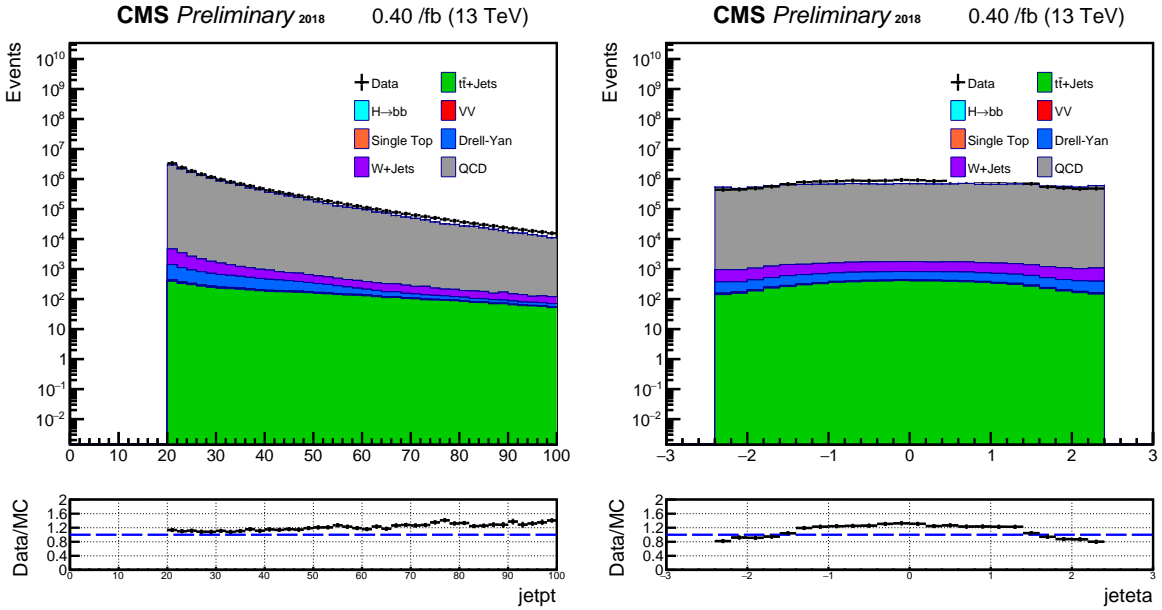
5.3 Taus

The analysis sources PAT::slimmedTaus from MINIAOD for MC and RECO::slimmedTaus for Data to produce `selectedTaus`. τ leptons have a 64% branching ratio to hadrons. The Hadron-Plus-Strip (HPS) algorithm enables the reconstruction of a τ lepton's hadronic decay. HPS uses PFJets as its starting point. τ's hadronic decay can be reconstructed with PFJets' charged hadrons in HCAL and 2 γs from π^0 decays in ECAL. Tau objects require

- pt $\geq$ 20 GeV

- $|\eta| \leq 2.4$

Figure 5.3: Data/MC of tau objects
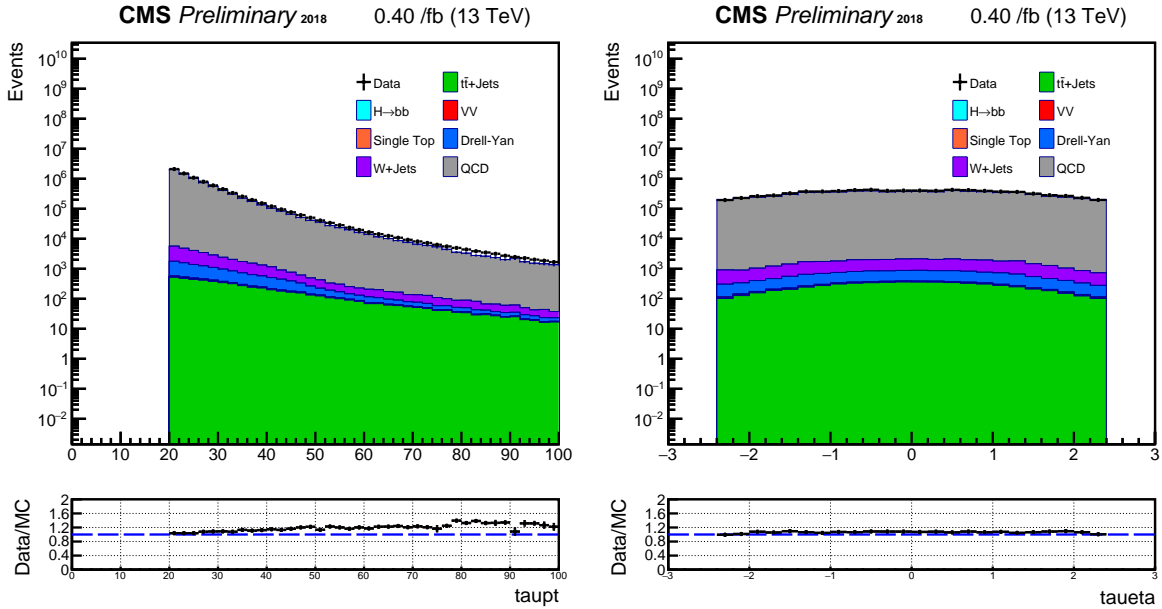
5.4 Region of Interest

The complete reconstruction procedure of Regions of Interest is detailed in the following subsections. An ROI requires

- Good quality track selection

- Vertex Fitted from pair-wise tracks by V0Fitter in CMSSW

- Cluster the fitted vertices to form a Region of Intrest (ROI)

- Look for tracks around $\Delta R = 0.3$ around ROI to save its isolation information

16

5.4.1 Tracks

The analysis sources packedPFCandidates and lostTracks from MINIAOD. Track parameters and convariance values will be propagated along the ROI production process and no value should be non-physical

- !isinf(tracks.parameter) and !isnan(tracks.parameter)

- !isinf(tracks.covariance) and !isnan(tracks.covariance)

- Number of valid hits > 3

- pt ≥ 0.35

- Track $IPSig_{XY}$ $\geq$2.

- Track $IPSig_Z$ $\geq$-1.

- Track normalized χ^2 $\geq$10.

5.4.2 Vertex Fitter

The analysis sources offlineBeamspot from MINIAOD for beamspot reference. Vertex fitter is KalmanVertexFitter with vertex cuts as below.

- Vertex χ^2 $\geq$6.63

- Transverse Decay distance significance$\geq$15.

- V0mass $\geq$13000GeV

- $\cos(\theta_{XY})$ between x and p of V0 candidate ≥ 0

- $\cos(\theta_{XYZ})$ between x and p of V0 candidate $\geq$ -2

5.4.3 ROI formation

Fitted vertices are clustered to form a Region of Interest (ROI). These ROIs have cuts on their parameters as below.

- Radius of ROI ≥ 1 cm

- Annulus $\Delta R \leq 0.3$

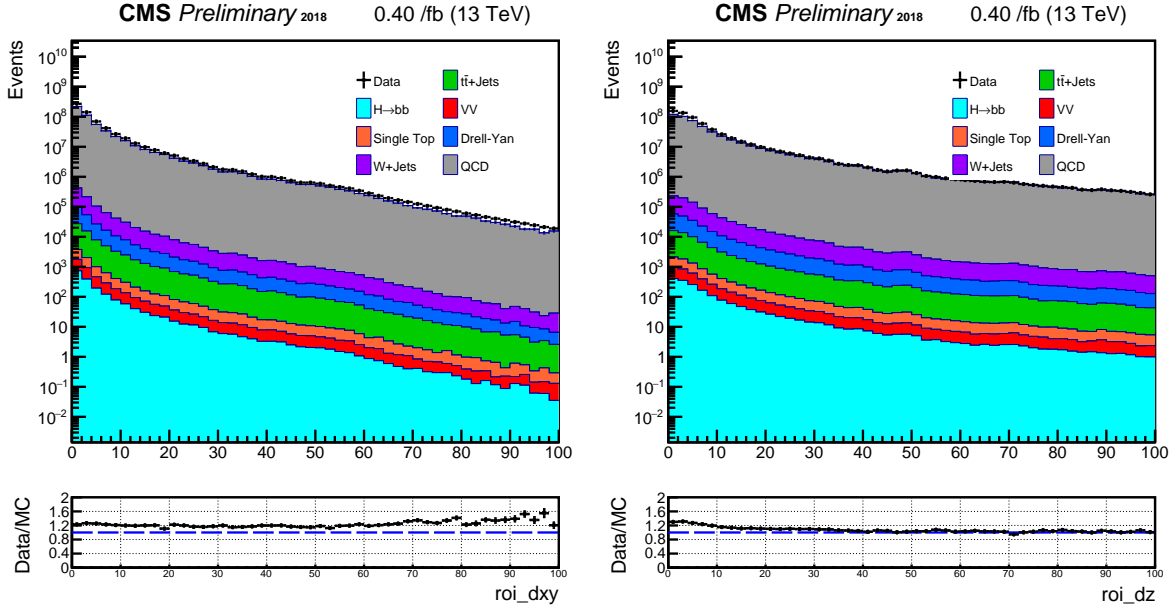Figure 5.4: Data/MC of ROI distribution

Figure 5.5: 2Data/MC of ROI distribution
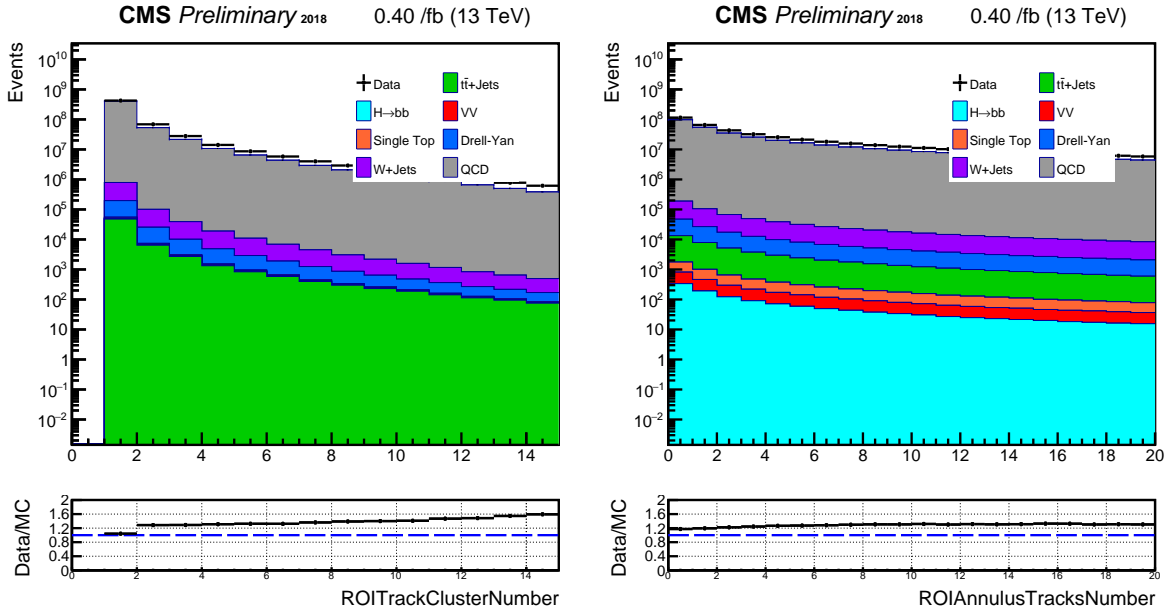
5.5 Pileup Reweighting

Pileup (PU) weight values are calculated for each era of data-taking (A,B,C,D). The data's number of Pileup events is accessed for the specific HLT path with the following commands

```
brilcalc lumi --byls --normtag
/cvmfs/cms-bril.cern.ch/cms-lumi-pog/Normtags/normtag_PHYSICS.json
-i processedLumis.json --hltpath HLT_Mu9_IP6_part0_v* -o output.csv
```

Please note that we get luminosity for the specific BPH HLT path and save the output for

pileupReCalc_HLTpaths.py

```
pileupReCalc_HLTpaths.py -i output.csv
--inputLumiJSON pileup_latest.txt -o My_HLT_corrected_PileupJSON.txt
--runperiod Run2
```

where, pileup_latest.txt is from

```
/afs/cern.ch/cms/CAF/CMSCOMM/COMM_DQM/certification/Collisions18/
13TeV/PileUp/pileup_latest.txt
```

Then, we substitute the usual pileup_latest.txt to My_HLT_corrected_PileupJSON.txt to obtain

the PU distribution of data.

```
pileupCalc.py -i processedLumis.json
--inputLumiJSON My\_HLT\_corrected\_PileupJSON.txt
--calcMode true --minBiasXsec 69200 --maxPileupBin 120 --numPileupBins 120
MyDataPileupHistogram.root
```

Figure 5.6 shows the BPH1-Era A's HLT_Mu9_IP6 HLT path's Data PU distribution.

Figure 5.6: ww
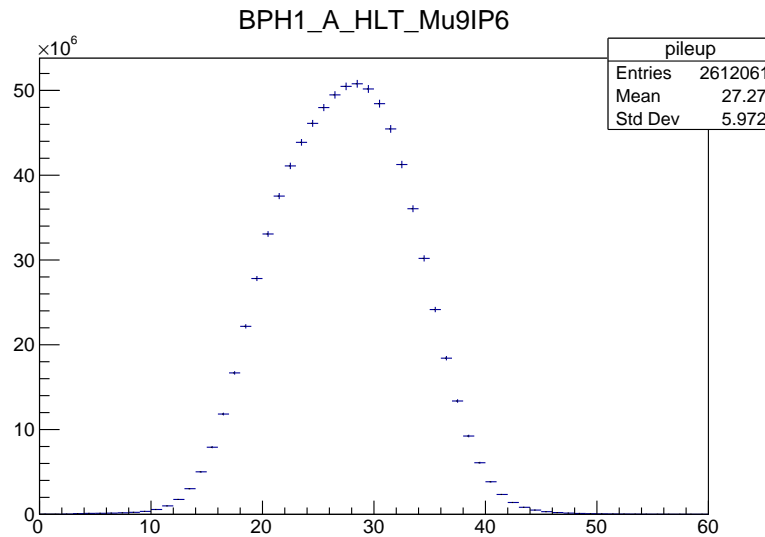
Figure 5.7 shows the BPH1-Era C's HLT_Mu12_IP6 HLT path's Data PU distribution.

19

Figure 5.7: dd
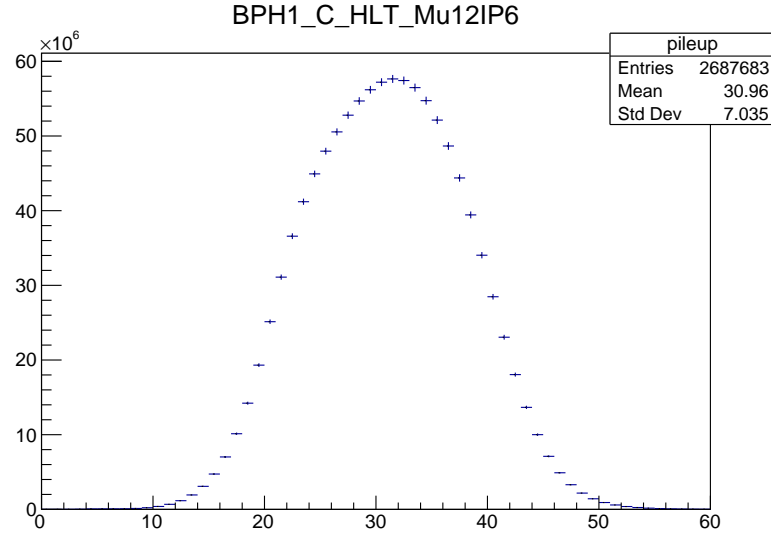
Figure 5.8: ed
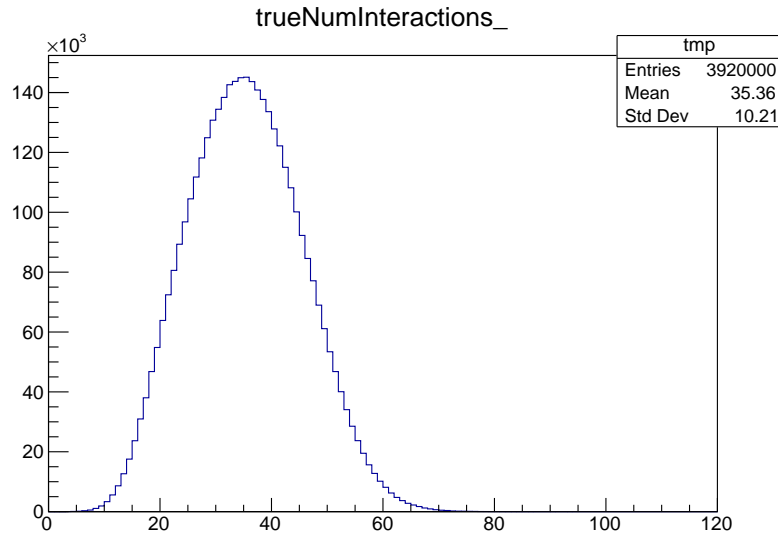
Figure 5.8 shows DYJetsToLL_M-50_TuneCP5_13TeV-madgraphMLM-pythia8 MC PU distribution.

With histograms above, one can create a PUWeight histogram distribution for an era's specific HLT path with commands below.

Figure 5.9 shows resultant such PUWeight from BPH1_A HLT_Mu9_IP6 and DYJetsToLL_M-50_TuneCP5_13TeV-madgraphMLM-pythia8.

Figure 5.9: aaaa
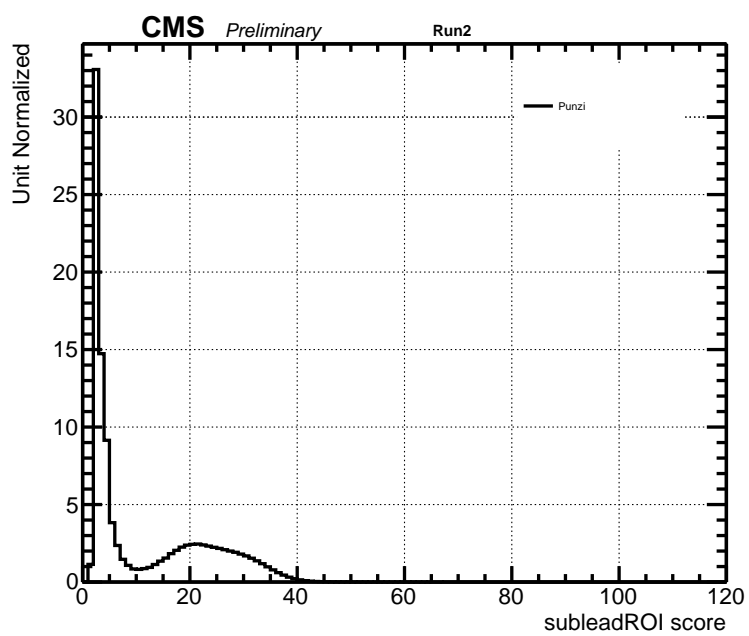
CHAPTER 6

MACHINE LEARNING

ROIs are artificial regions created by the CMSSW mechanism, which are displaced vertex candiates. ROIs contain thorough information about fitted tracks, vertices, and isolation information, after following the formation procedure described in the previous section. The exhaustive variables saved in each ROI contain information, which directly and indirectly tells whether the ROI is from signal process or background process. Given the extensive amount of variables within ROIs, it's inappropriate to use ROIs' single or a few variabes as our tagging variables, like in ZH analysis [45]. It is also ineffcient to implement a cut-based approach due to having approximately 20-30 variables from ROI. Optimization process for all 20-30 variables would be extremley time-consuming, inefficient, and error-prone as well. Therefore, the analysis exploits machine learning (ML) for these multivariate analysis. Boosted decision trees will also face similar problem as cut-based analysis, although to a lesser extent. Deep Neural Network are the most adaptable ML algorithm for this analysis method, in which the analysis inputs extensive list of ROI variables into a neural network, and receives a final score to discriminate ROIs that arise in signal process versus background processes.

6.1   Machine Leaning Software

The analysis uses Keras-Tensorflow via CMSSW. CMSSW includes Keras-Tensorflow, which enables simple and easy usage of keras-Tensorflow with simple cmsenv command in various CMS remote clusters. For CMSSW_10_6_12 (to have access for BPH trigger path), Keras-Tensorflow version is 2.3.1. It runs with CPUs and GPUs. CMSSW includes image container for Keras-Tensorflow and researchers can submit remote batch jobs for its ML training. The analysis tested multiple variables (such as epoch numbers, batch sizes, phi sizes, f sizes) of our DNN layers thanks to submission of remote batch jobs with CMSSW's Keras-Tensorflow image container. Subsection 6.3 below details the numerical results from such tests. The analysis also tested different combinations of signal vs background datasets for maximum discriminant power. The list of mass scale and lifetime tested for signal points are listed in subsection 6.4. Different SM physics process (and their

compositions) tested for background process are also listed in subsection 6.4 The analysis used the tensorflow protocol buffer files, which were trained with parameters and physics process as in Table 6.1.

Table 6.1: Tensorflow information

Epoch	300
batch size	250
Phi sizes	((64,128,256),(32,64,128))
f sizes	(256,128,32)
Signal	ggHSSTo4Tau-MS15GeV-cτ100mm
Background	QCD_Pt120-170_MuEneriched and TTJets

6.2   Machine Learning Input Variable

The extensive variables for input of our DNN are described and categorized in Tables 6.2, 6.3, and 6.4.

Table 6.2: ROI (trackCluster) variables by category

TrackCluster	Position	TrackClusters.vx() - primaryVertex.X()
	Position	TrackClusters.vy() - primaryVertex.Y()
	Position	TrackClusters.vz() - primaryVertex.Z()
	Covariance	TrackClusters.vertexCovariance()(0,0)
	Covariance	TrackClusters.vertexCovariance()(0,1)
	Covariance	TrackClusters.vertexCovariance()(0,2)
	Covariance	TrackClusters.vertexCovariance()(1,0)
	Covariance	TrackClusters.vertexCovariance()(1,1)
	Covariance	TrackClusters.vertexCovariance()(1,2)
	Track0,1	Track0,1.pt
	Track0,1	Track0,1.eta
	Track0,1	Track0,1.phi
	Track0,1	Track0,1.dxy
	Track0,1	Track0,1.dz
	Track0,1	Track0,1.normalizedChi2
	Track0,1	Track0,1.HighPurityInt

6.3   DNN Variable Test

For Ethan.

Table 6.3: ROI (Annulus) variables by category

Annulus	pfCandidate/LostTracks	pfCandidate/LostTracks.pt
	pfCandidate/LostTracks	pfCandidate/LostTracks.eta
	pfCandidate/LostTracks	pfCandidate/LostTracks.phi
	pfCandidate/LostTracks	pfCandidate/LostTracks.dxy
	pfCandidate/LostTracks	pfCandidate/LostTracks.dz
	pfCandidate/LostTracks	pfCandidate/LostTracks.normalizedChi2
	pfCandidate/LostTracks	pfCandidate/LostTracks.HighPurityInt
	pfCandidate/LostTracks	pfCandidate/LostTracks.DeltaR(trackMomentum)

Table 6.4: Event variables by category

ROI	Position	x
	Position	y
	Position	z

Figure 6.1: asdasdasd
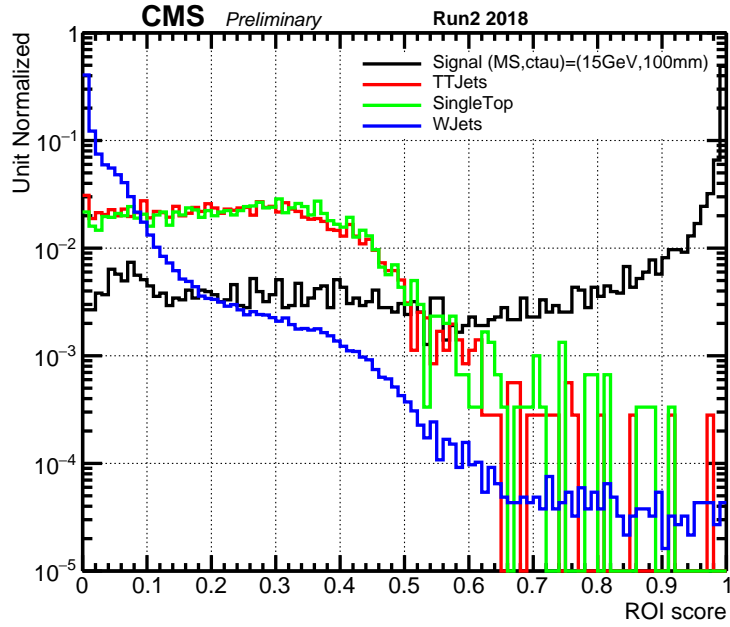
6.4   Signal and Background MC Test

For Ethan.

Figure 6.2: Data/MC agreement for ROI scores

6.5 SHAP values

For Ethan.

Figure 6.3: Data/MC agreement for loglead/sublead scroes

CHAPTER 7

EVENT SELECTION, SIGNAL AND CONTROL REGIONS

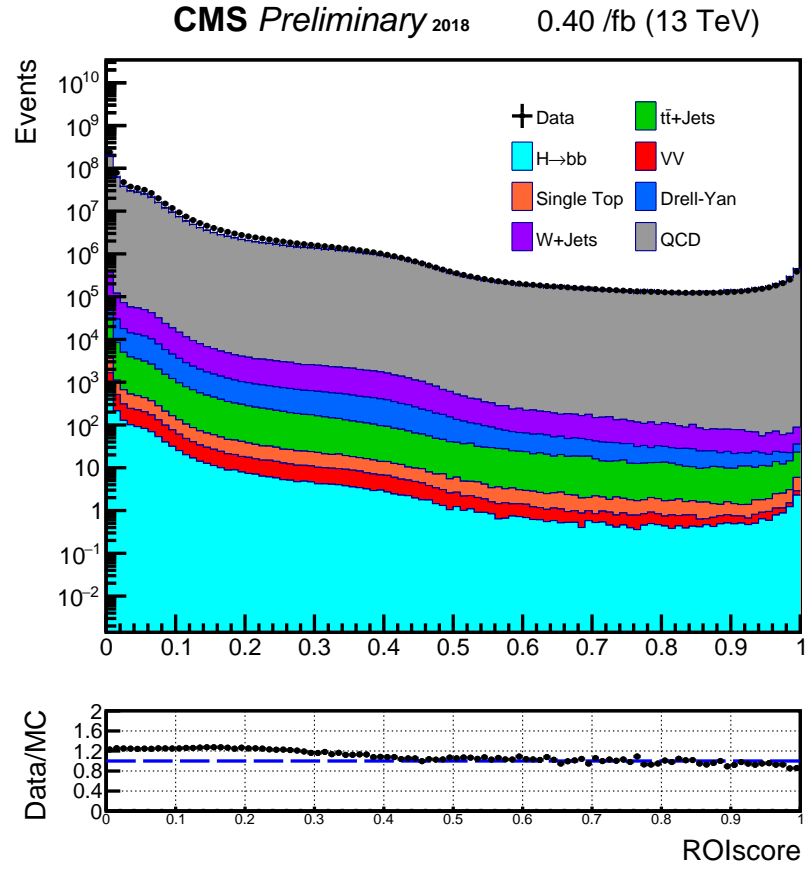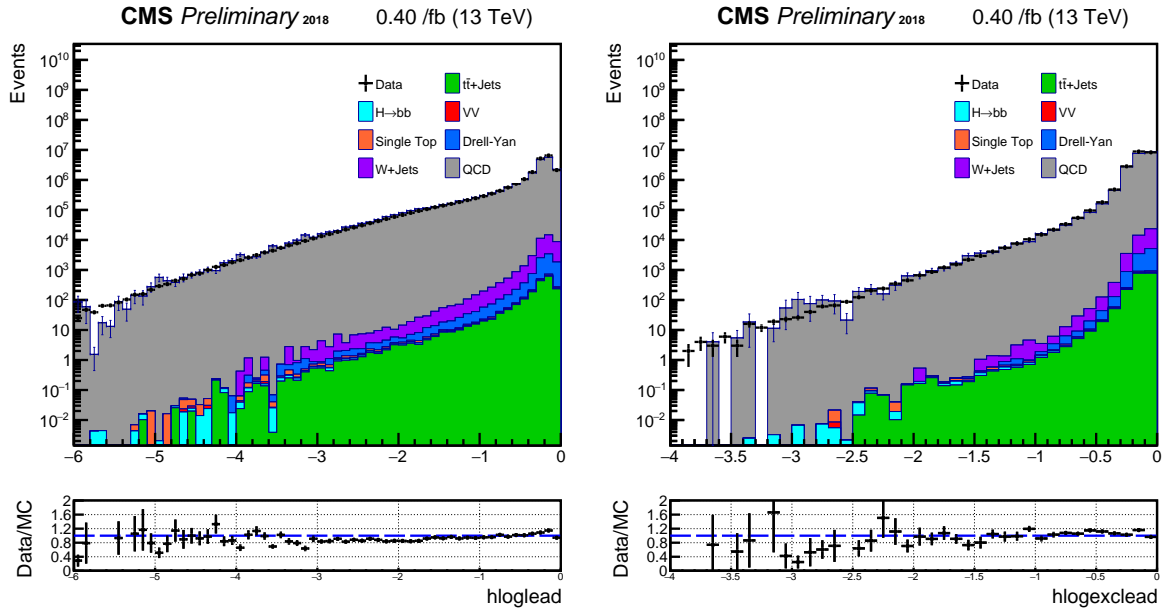ROIs of all events inside the dataset listed in section **??** are scored with the tensorflow, process trained with information from section 6.2. Given that the signal process has 2 scalar decays as in Figure A.1, it's reasonable to require 2 high-scoring ROIs for our analysis. (However, the 2 selected ROIs are not simply the 2 highest-scoring ROIs of the event, due to non-negligible lifetime of τ leptons (from signal process) in the detector. The cuts on the leading ROI, and the subleading ROI are optimized based on maximizing the punzi significance formula with value σ set to discovery value of 5.

$$\sigma(N_{\text{displaced}-\text{tag}}) = \frac{S(N_{\text{displaced}-\text{tag}})}{\sqrt{B(N_{\text{displaced}-\text{tag}}) + 2.5}}. \tag{7.1}$$

Figure 7.1: Signal versus Background for log10(1-ROIscore), where the ROI score is the highest ROI of the event. Left plot is for MS-15_ctauS-10mm point, whereas the right plot is for MS-15_cauS-100mm point
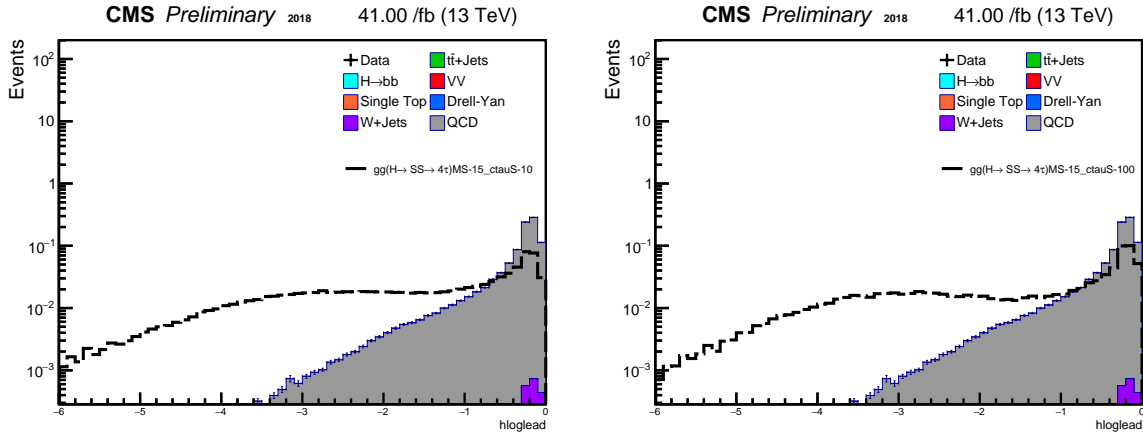
In addition, we have other cuts applied throughout the analysis. These variables are either

- Non-relevant to ROIs (muon, jet object)

- Construction of geometric variable after selecting 2 highest scoring ROIs.

- Missing input variable in ROI training

27

Figure 7.2: Signal versus Background for log10(1-subROIscore), where the ROI score is the second highest ROI (outside of dPhi=0.4 from leading ROI) of the event. Left plot is for MS-15_ctauS-10mm point, whereas the right plot is for MS-15_cauS-100mm point
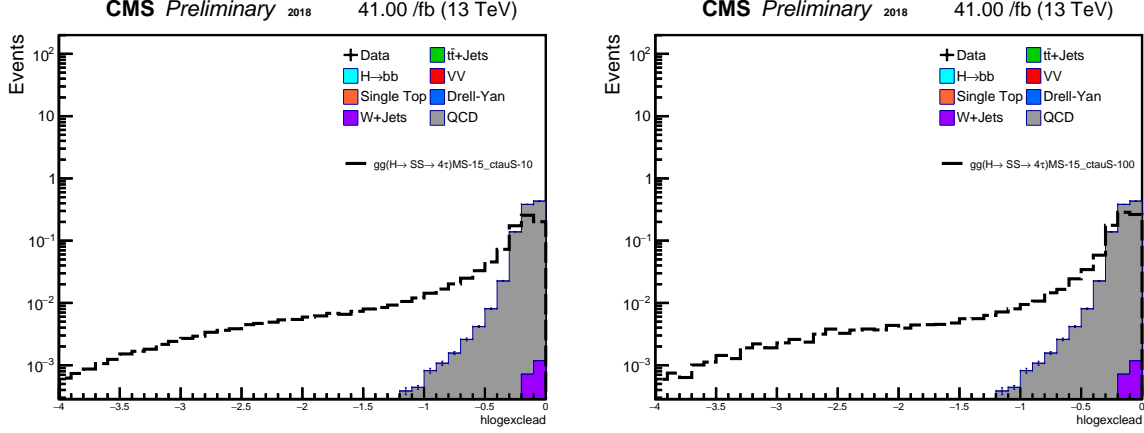
These are not inputs of ML training, something that can't be learned by the ML, so not discriminated with scoring of the ROIs.

They include

- $\Delta\Phi(leadROI, subleadROI)$

- Number of Annulus tracks associated with ROI < 8

- 1 Isolated μ

- $\Delta R(leadROI, Jet) <$0.6

- Leading μ's transverse impact parameter to PV > 0.1

Each of the cuts for the items above is motivated and explained in following subsections.

7.1 Delta Phi(lead ROI,sublead ROI)

This analysis looks for displaced vertices in the tracker region, coming from the decays of exotic LLPs from Higgs produced in gluon fusion mode, leaving the SM Higgs boson without boost. The largest mass of the exotic LLPs is 55 GeV, ranging down to 7 GeV. Thus, exotic LLPs decayed from the SM Higgs become boosted, with their momentum vectors pointing back-to-back in the SM Higgs rest frame. Exotic LLPs with lighter mass are more boosted than heavier LLPs, since less LLP mass means more leftover energy into kinetic energy. Given that ROIs corresponding

28

to an exotic LLP's decay should have the highest ROI score, one should expect that the leading ROI and subleading ROI in a single event would be back-to-back. Thus, in signal events, $\Delta\Phi$(lead ROI,sublead ROI) tends to have high values, while the background processes tend to have a more uniform distribution. This analysis applies a cut above 2.2 to reduce background contribution. Optimization process for this variable is detailed in here (To be done in future?)

Figure 7.3: Signal versus Background for Delta Phi(leadROI, subleadROI). Left plot is for MS-15_ctauS-10mm point, whereas the right plot is for MS-15_cauS-100mm point
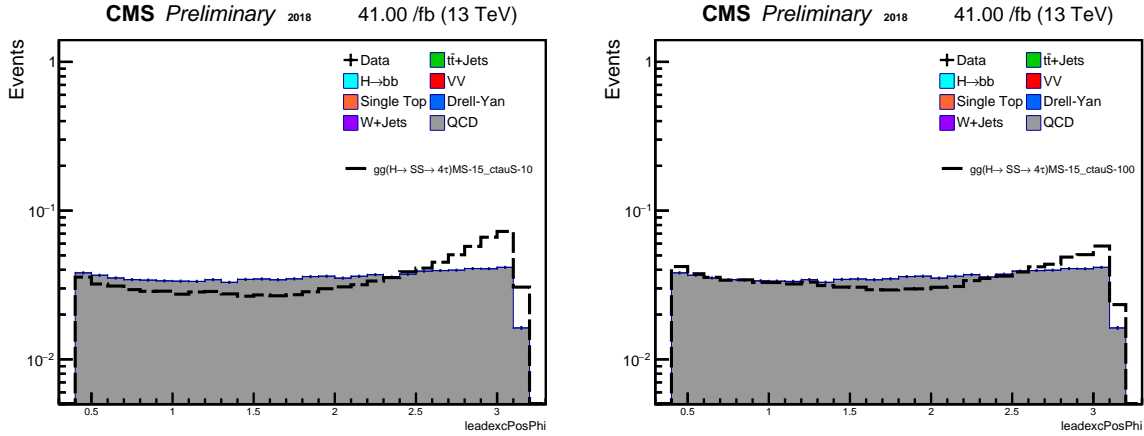
7.2 Number of Annulus Tracks Associated with ROI

The tensorflow used for this analysis is trained with p_T, η, χ^2, and other information of the annulus tracks (tracks that are inside ROI radius, but not fitted to vertex). Meanwhile, an ROI's total number of annulus tracks is not a direct input for ML and tensorflow can only learn such information indirectly via annulus tracks' p_T. Although having selected ROIs with high scores (>0.999), signal processes ROIs' number of annulus tracks show a quite different distribution from the background process. signal's high-scoring ROIs are mostly from the the exotic LLP scalar's decay into τ leptons. Since the signal's high-score ROIs' are very well isolated, the ROI's number of annulus tracks is very low. QCD background events, which are our dominant background, have a poor isolation quality. Since QCD's high-scoring ROI's are poorly isolated due to QCD nature, these ROIs' numbers of annulus tracks are higher than the signal. More precisely, QCD's high-scoring ROI's are usually from B-mesons, which have higher track multiplicity than τ leptons.

Figure 7.4: Number of tracks in the annulus cone of the leading ROI. Left plot is for MS-15_ctauS-10mm point, whereas the right plot is for MS-15_cauS-100mm point
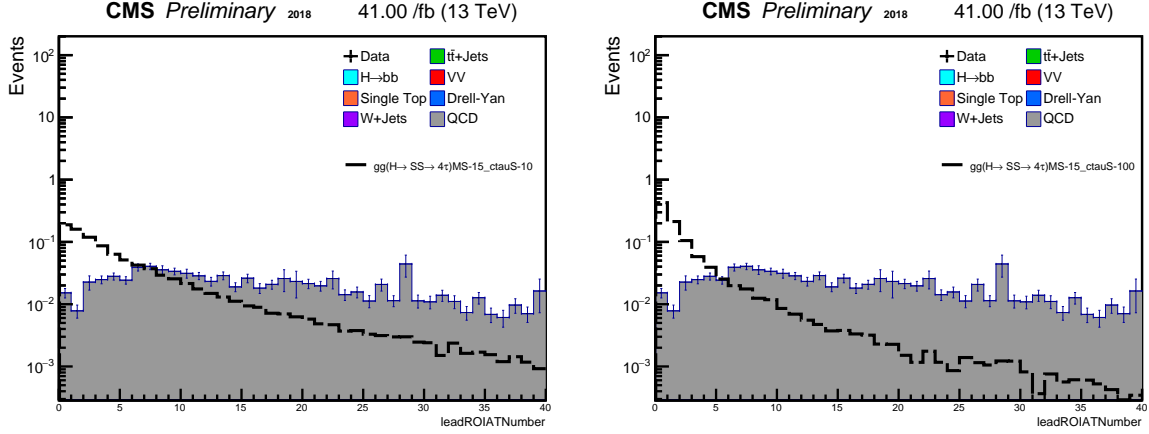
7.3 Isolation criteria for muons

Leptonic decay of B-meson generates muons, which trigger the B-parking trigger of the analysis. Muons of B-meson decay have very poor isolation quality, just like ROIs formed around the B-meson decay. In contrast, muons of τ lepton decay have better isolation quality. In order to eliminate the dominant B-meson background from the QCD process, the analysis applies a PFISOLoose in selecting muon objects. The precise definition of PFISOLoose is defined as below.

- $(\Sigma pT(ch.had from PV) + max(0, \Sigma ET(neut.had)\Sigma ET(phot) - 0.5*\Sigma pT(ch.had from PU)))/P_T(\mu) <$ 0.25

Some muons decayed from τ lepton with 7 GeV mass fail isolation cut, due to its poorer isolation quality from the boost. However, it still benefits to apply the PFISOLoose cut on muons given it removes more background events than signal events. The table below demonstrates event yield drop before and after requiring PFISOLoose cut on muons, classified by its signal and background process.

7.4 Leading muon's transverse impact parameter to PV

With the B-Parking trigger, triggering muons have significant transverse displacement (impact parameter) in both background and signal processes. However, displacement in the signal process is greater than the that of the background process. The signal process has at minimum of $c\tau =$ 1mm, which is longer than B-meson lifetime. Thus, triggering muon object's transverse impact

parameter to PV is larger in signal process than background process. The analysis implements a cut on this variable.

Figure 7.5: leading muon's transverse impact parameter value to the primary vertex. Left plot is for MS-15_ctauS-10mm point, whereas the right plot is for MS-15_cauS-100mm point
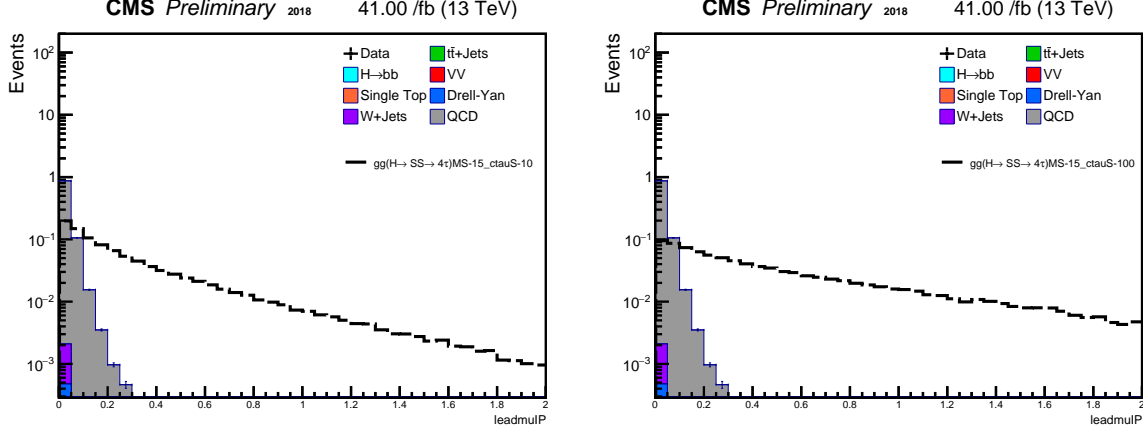
7.5   DeltaR(ROI, jet)

τ leptons of the signal process can also decay hadronically, while only one of the τ leptons decay muonically to trigger B parking trigger. When τ leptons decay hadronically, its decay shower can get clustered in the calorimeter, and reconstructed as a jet. Given the τ lepton's on-shell mass is a fixed value, τ lepton and its hadronic decay products (to-be clustered into a jet) have a specific kinematic phase space. Thus, the Δ R(ROI, jet) has a distribution with a peak at a certain value (around 0.3-0.6). Meanwhile, the QCD backround has a different distribution shape. Given the hadronic nature of the process, jet multiplicity is high. Higher jet multiplicity makes the Δ R(ROI,jet) value to have a rather randomized value, resulting in a flat distribution.

Figure 7.6: Delta R(Jet, leadingROI). Left plot is for MS-15_ctauS-10mm point, whereas the right plot is for MS-15_cauS-100mm point
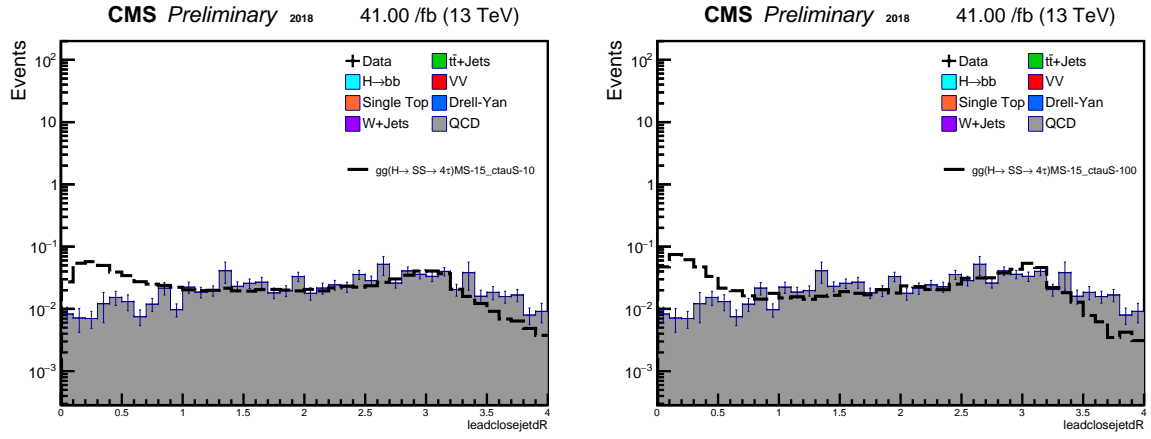
CHAPTER 8

BACKGROUND ESTIMATION

Section 7 listed seven different discriminant variables for the analysis. Leading ROI score, subleading ROI score, and leading muon's IP value have the most discriminatory power. The analysis uses data-driven background estimation method and an ABCD method is the most preferred thanks to its simplicity. However, leading ROI score and subleading ROI score are correlated in the QCD background process. ROIs from B-mesons score higher in our tensorflow. In QCD processes, the B-mesons are likely to be pair produced. Therefore, when the leading ROI score is high due to its b-like behavior, the sublead ROI score is also high because the anti-meson is produced on the other side of the detector. Thus, leading and sublead scores can't be our ABCD discriminant variable candidates du to their correlation.

The analysis selects leading ROI and leading muon's IP value as its ABCD discriminant variables. After implementing all other cuts (sublead ROI, $\Delta\Phi(lead, sublead)$, Number of Annulus tracks associated with ROI, 1 Isolated μ, $\Delta R(leadROI, Jet)$), we tested the correlation factor between the leading ROI, and leading mu's IP values for each background process. The values are pretty minimal except for 2-3 processes where there were too few entries to derive a physical conclusion due to statistical limitations. Therefore, the analysis uses leading muIP and leading ROI score for its ABCD discriminant variables.

The results are listed below.

Figure 8.1: Cutflow histogram of MS15GeV-ct100mm point. Left plot is for region A, whereas the right plot is for region D
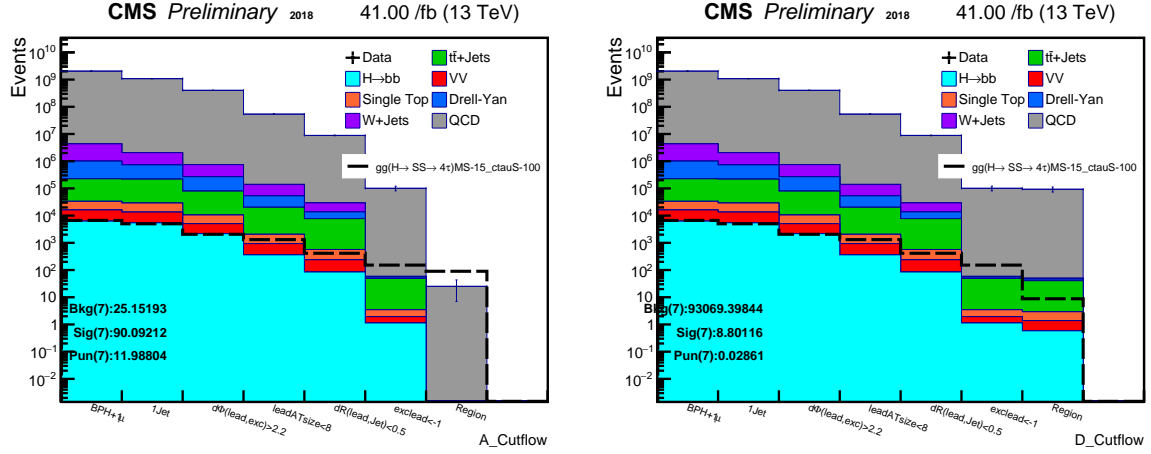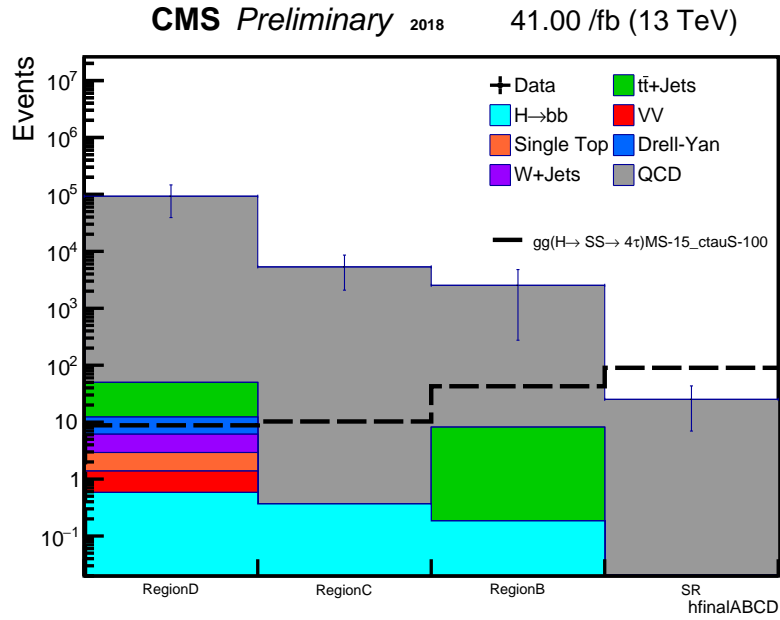

Figure 8.2: eee

CHAPTER 9

SYSTEMATIC UNCERTAINTIES

About systematic Uncertainty

CHAPTER 10

RESULTS
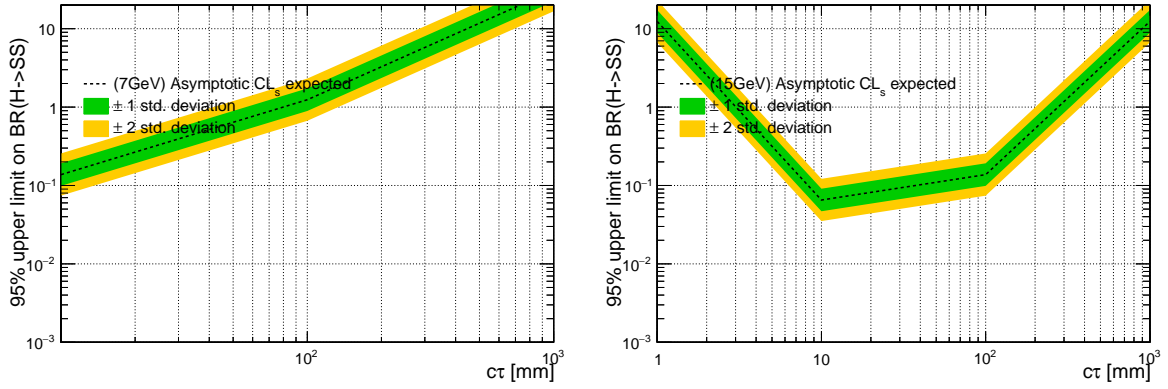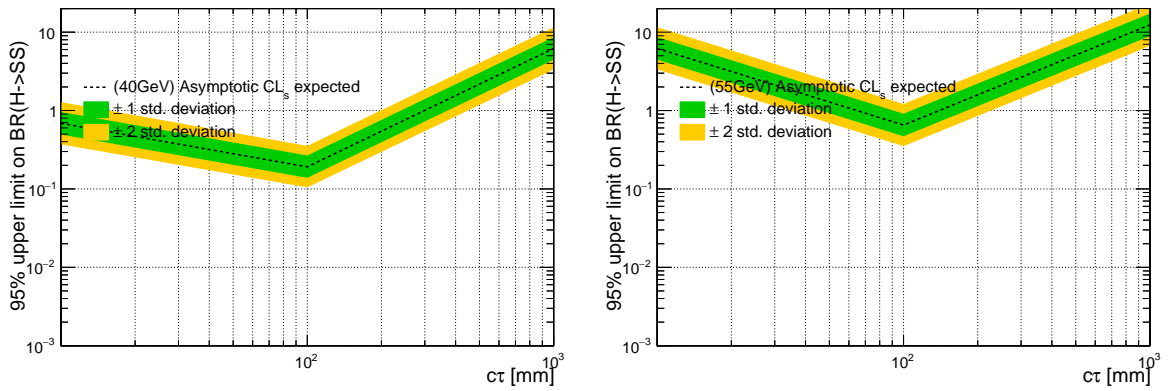
Results

Figure 10.1: Current Preliminary limit plots

Figure 10.2: Current Preliminary limit plots

CHAPTER 11

CONCLUSIONS

This was an interesting analysis targeting tau lepton final state with tracker lifetime

APPENDIX A

DATA SAMPLES

This appendix is here merely to demonstrate how appendices may be included and formatted in your document. Look through the files `thesis.tex` and `appendix.tex` to see how these pieces work together.

The analysis uses B Parking datasets. Data was collected during the 2018 portion of Run 2 and corresponds to an integrated luminosity of 50 fb^{-1}.

Table A.1: Datasets used in the analysis

Data sample	Integrated Luminosity (fb$^-$1)
/ParkingBPH1/Run2018A-05May2019-v1/MINIAOD	0.866
/ParkingBPH2/Run2018A-05May2019-v1/MINIAOD	0.866
/ParkingBPH3/Run2018A-05May2019-v1/MINIAOD	0.866
/ParkingBPH4/Run2018A-05May2019-v1/MINIAOD	0.866
/ParkingBPH5/Run2018A-05May2019-v1/MINIAOD	0.866
/ParkingBPH6/Run2018A-05May2019-v1/MINIAOD	0.866
Total	5.20
/ParkingBPH1/Run2018B-05May2019-v2/MINIAOD	1.083
/ParkingBPH2/Run2018B-05May2019-v2/MINIAOD	1.083
/ParkingBPH3/Run2018B-05May2019-v2/MINIAOD	1.083
/ParkingBPH4/Run2018B-05May2019-v2/MINIAOD	1.083
/ParkingBPH5/Run2018B-05May2019-v2/MINIAOD	1.083
/ParkingBPH6/Run2018B-05May2019-v2/MINIAOD	1.083
Total	6.49
/ParkingBPH1/Run2018C-05May2019-v1/MINIAOD	1.079
/ParkingBPH2/Run2018C-05May2019-v1/MINIAOD	1.079
/ParkingBPH3/Run2018C-05May2019-v1/MINIAOD	1.079
/ParkingBPH4/Run2018C-05May2019-v1/MINIAOD	1.079
/ParkingBPH5/Run2018C-05May2019-v1/MINIAOD	1.079
Total	5.39
/ParkingBPH1/Run2018D-05May2019promptD-v1/MINIAOD	6.542
/ParkingBPH2/Run2018D-05May2019promptD-v1/MINIAOD	6.542
/ParkingBPH3/Run2018D-05May2019promptD-v1/MINIAOD	6.542
/ParkingBPH4/Run2018D-05May2019promptD-v1/MINIAOD	6.542
/ParkingBPH5/Run2018D-05May2019promptD-v1/MINIAOD	6.542
Total	32.7
ParkingBPH Total	50.78

A.1   Monte Carlo Samples

A.1.1   Signal Model and Simulation

The ggH production process (see Figure A.1) is generated at next-to-next-to-leading order (NNLO) and next-to-next-to-leading-log (NNLL) QCD and next-to-leading order (NLO) EW accuracies [56]. The Higgs boson mass is set to 125GeV for all signal samples. The cross sections, computed at NNLO+NNLL QCD and NLO EW accuracies and obtained from CERN Yellow Report 3, are 4.414 pb. The CMS detector response is modeled with GEANT4 [57].

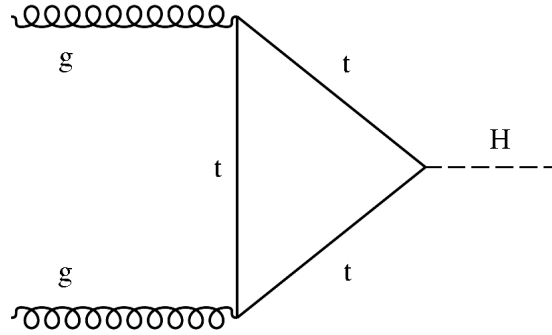Figure A.1: Leading Feynman diagrams for ggH production mode

Table A.1.1 lists the signal Monte Carlo samples.

Sample
/ggH_HToSSTo4Tau_MH-125_TuneCP5_13TeV-powheg-pythia8/CAMPAIGN/MINIAODSIM
/ggH_HToSSTo4Tau_MH-125_MS-55_ctauS-1_TuneCP5_13TeV-powheg-pythia8/CAMPAIGN/MINIAODSIM
/ggH_HToSSTo4Tau_MH-125_MS-55_ctauS-10_TuneCP5_13TeV-powheg-pythia8/CAMPAIGN/MINIAODSIM
/ggH_HToSSTo4Tau_MH-125_MS-55_ctauS-100_TuneCP5_13TeV-powheg-pythia8/CAMPAIGN/MINIAODSIM
/ggH_HToSSTo4Tau_MH-125_MS-55_ctauS-1000_TuneCP5_13TeV-powheg-pythia8/CAMPAIGN/MINIAODSIM
/ggH_HToSSTo4Tau_MH-125_MS-40_ctauS-1_TuneCP5_13TeV-powheg-pythia8/CAMPAIGN/MINIAODSIM
/ggH_HToSSTo4Tau_MH-125_MS-40_ctauS-10_TuneCP5_13TeV-powheg-pythia8/CAMPAIGN/MINIAODSIM
/ggH_HToSSTo4Tau_MH-125_MS-40_ctauS-100_TuneCP5_13TeV-powheg-pythia8/CAMPAIGN/MINIAODSIM
/ggH_HToSSTo4Tau_MH-125_MS-40_ctauS-1000_TuneCP5_13TeV-powheg-pythia8/CAMPAIGN/MINIAODSIM
/ggH_HToSSTo4Tau_MH-125_MS-15_ctauS-1_TuneCP5_13TeV-powheg-pythia8/CAMPAIGN/MINIAODSIM
/ggH_HToSSTo4Tau_MH-125_MS-15_ctauS-10_TuneCP5_13TeV-powheg-pythia8/CAMPAIGN/MINIAODSIM
/ggH_HToSSTo4Tau_MH-125_MS-15_ctauS-100_TuneCP5_13TeV-powheg-pythia8/CAMPAIGN/MINIAODSIM
/ggH_HToSSTo4Tau_MH-125_MS-15_ctauS-1000_TuneCP5_13TeV-powheg-pythia8/CAMPAIGN/MINIAODSIM
/ggH_HToSSTo4Tau_MH-125_MS-7_ctauS-1_TuneCP5_13TeV-powheg-pythia8/CAMPAIGN/MINIAODSIM
/ggH_HToSSTo4Tau_MH-125_MS-7_ctauS-10_TuneCP5_13TeV-powheg-pythia8/CAMPAIGN/MINIAODSIM
/ggH_HToSSTo4Tau_MH-125_MS-7_ctauS-100_TuneCP5_13TeV-powheg-pythia8/CAMPAIGN/MINIAODSIM
/ggH_HToSSTo4Tau_MH-125_MS-7_ctauS-1000_TuneCP5_13TeV-powheg-pythia8/CAMPAIGN/MINIAODSIM

A.1.2   Background Monte Carlo

All samples were processed as recommended in the PPD Run2 Analysis Guideline [58]. Tables A.2-A.5 summarizes the background Monte Carlo used in this analysis.
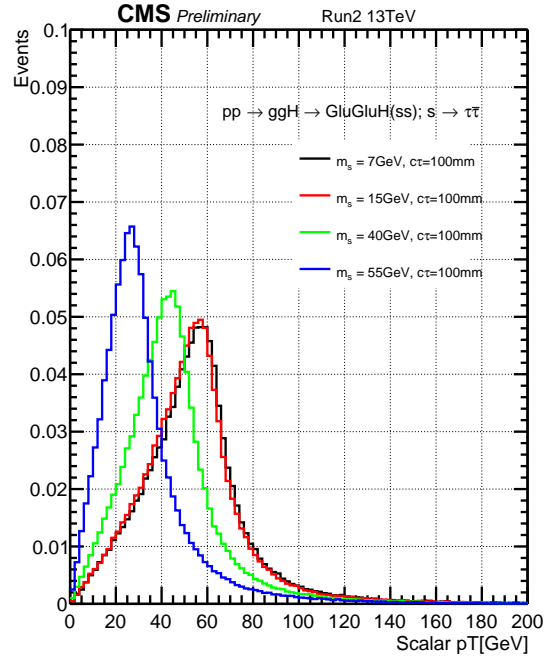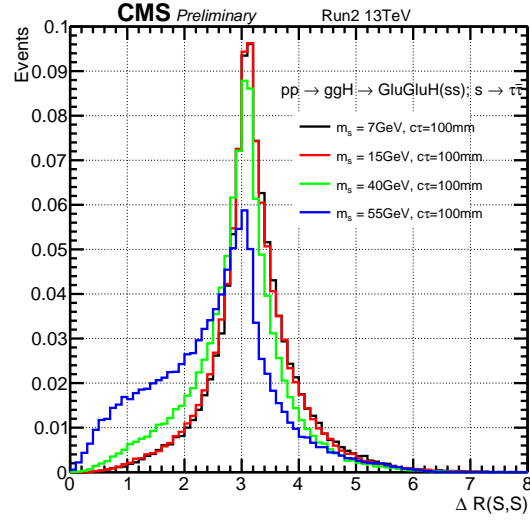
Figure A.2: pt of the scalar products

Figure A.3: DeltaR of the scalar products

a

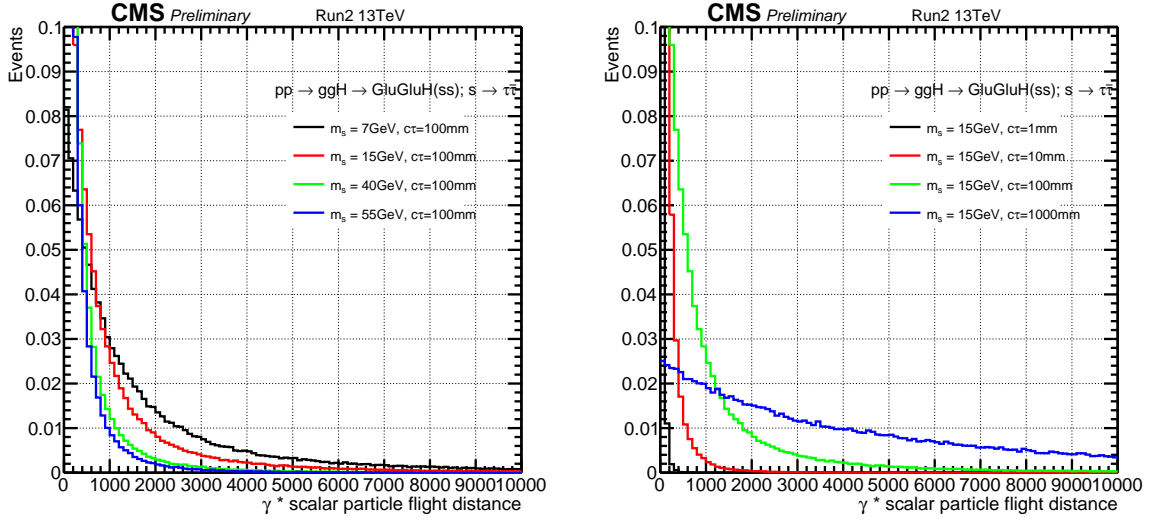Figure A.4: liftime of the scalar products in the lab frame

Table A.2: QCD MuEnriched Pt5 background Monte Carlo samples

Sample
/QCD_Pt-15to20_MuEnrichedPt5_TuneCP5_13TeV_pythia8/*-v3/MINIAODSIM
/QCD_Pt-20to30_MuEnrichedPt5_TuneCP5_13TeV_pythia8/*-v4/MINIAODSIM
/QCD_Pt-30to50_MuEnrichedPt5_TuneCP5_13TeV_pythia8/*-v3/MINIAODSIM
/QCD_Pt-50to80_MuEnrichedPt5_TuneCP5_13TeV_pythia8/*-v3/MINIAODSIM
/QCD_Pt-80to120_MuEnrichedPt5_TuneCP5_13TeV_pythia8/*_ext1-v2/MINIAODSIM
/QCD_Pt-120to170_MuEnrichedPt5_TuneCP5_13TeV_pythia8/*_ext1-v2/MINIAODSIM
/QCD_Pt-170to300_MuEnrichedPt5_TuneCP5_13TeV_pythia8/*-v3/MINIAODSIM
/QCD_Pt-300to470_MuEnrichedPt5_TuneCP5_13TeV_pythia8/*_ext3-v1/MINIAODSIM
/QCD_Pt-470to600_MuEnrichedPt5_TuneCP5_13TeV_pythia8/*_ext1-v2/MINIAODSIM
/QCD_Pt-600to800_MuEnrichedPt5_TuneCP5_13TeV_pythia8/*-v1/MINIAODSIM
/QCD_Pt-800to1000_MuEnrichedPt5_TuneCP5_13TeV_pythia8/*_ext3-v2/MINIAODSIM
/QCD_Pt-1000toInf_MuEnrichedPt5_TuneCP5_13TeV_pythia8/*-v1/MINIAODSIM

Table A.3: W,Z,H boson background Monte Carlo samples

Sample
/DYJetsToLL_M-50_TuneCP5_13TeV-madgraphMLM-pythia8/*-v1/MINIAODSIM
/WJetsToLNu_M-50_TuneCP5_13TeV-madgraphMLM-pythia8/*-v2/MINIAODSIM
/WW_M-50_TuneCP5_13TeV-madgraphMLM-pythia8/*-v2/MINIAODSIM
/WZ_M-50_TuneCP5_13TeV-madgraphMLM-pythia8/*-v3/MINIAODSIM
/ZZ_M-50_TuneCP5_13TeV-madgraphMLM-pythia8/*-v2/MINIAODSIM
/GluGluHToBB_M125_13TeV_amcatnloFXFX_pythia8/*-v1/MINIAODSIM

Table A.4: Top background Monte Carlo samples

Sample
/TTJets_TuneCP5_13TeV-madgraphMLM-pythia8/*-v1/MINIAODSIM
/ST_s-channel_4f_hadronicDecays_TuneCP5_13TeV-madgraph-pythia8/*_ext1-v1/MINIAODSIM
/ST_t-channel_top_5f_TuneCP5_13TeV-powheg-pythia8/*-v1/MINIAODSIM
/ST_t-channel_antitop_5f_TuneCP5_13TeV-powheg-pythia8/*-v1/MINIAODSIM
/ST_tW_antitop_5f_inclusiveDecays_TuneCP5_13TeV-powheg-pythia8/*_ext1-v1/MINIAODSIM
/ST_tW_top_5f_inclusiveDecays_TuneCP5_13TeV-powheg-pythia8/*_ext1-v1/MINIAODSIM

Table A.5: Monte Carlo sample summary

Sample
/QCD_Pt-15to20_MuEnrichedPt5_TuneCP5_13TeV_pythia8/*-v3/MINIAODSIM
/QCD_Pt-20to30_MuEnrichedPt5_TuneCP5_13TeV_pythia8/*-v4/MINIAODSIM
/QCD_Pt-30to50_MuEnrichedPt5_TuneCP5_13TeV_pythia8/*-v3/MINIAODSIM
/QCD_Pt-50to80_MuEnrichedPt5_TuneCP5_13TeV_pythia8/*-v3/MINIAODSIM
/QCD_Pt-80to120_MuEnrichedPt5_TuneCP5_13TeV_pythia8/*_ext1-v2/MINIAODSIM
/QCD_Pt-120to170_MuEnrichedPt5_TuneCP5_13TeV_pythia8/*_ext1-v2/MINIAODSIM
/QCD_Pt-170to300_MuEnrichedPt5_TuneCP5_13TeV_pythia8/*-v3/MINIAODSIM
/QCD_Pt-300to470_MuEnrichedPt5_TuneCP5_13TeV_pythia8/*_ext3-v1/MINIAODSIM
/QCD_Pt-470to600_MuEnrichedPt5_TuneCP5_13TeV_pythia8/*_ext1-v2/MINIAODSIM
/QCD_Pt-600to800_MuEnrichedPt5_TuneCP5_13TeV_pythia8/*-v1/MINIAODSIM
/QCD_Pt-800to1000_MuEnrichedPt5_TuneCP5_13TeV_pythia8/*_ext3-v2/MINIAODSIM
/QCD_Pt-1000toInf_MuEnrichedPt5_TuneCP5_13TeV_pythia8/*-v1/MINIAODSIM
/DYJetsToLL_M-50_TuneCP5_13TeV-madgraphMLM-pythia8/*-v1/MINIAODSIM
/WJetsToLNu_M-50_TuneCP5_13TeV-madgraphMLM-pythia8/*-v2/MINIAODSIM
/WW_M-50_TuneCP5_13TeV-madgraphMLM-pythia8/*-v2/MINIAODSIM
/WZ_M-50_TuneCP5_13TeV-madgraphMLM-pythia8/*-v3/MINIAODSIM
/ZZ_M-50_TuneCP5_13TeV-madgraphMLM-pythia8/*-v2/MINIAODSIM
/GluGluHToBB_M125_13TeV_amcatnloFXFX_pythia8/*-v1/MINIAODSIM
/TTJets_TuneCP5_13TeV-madgraphMLM-pythia8/*-v1/MINIAODSIM
/ST_s-channel_4f_hadronicDecays_TuneCP5_13TeV-madgraph-pythia8/*_ext1-v1/MINIAODSIM
/ST_t-channel_top_5f_TuneCP5_13TeV-powheg-pythia8/*-v1/MINIAODSIM
/ST_t-channel_antitop_5f_TuneCP5_13TeV-powheg-pythia8/*-v1/MINIAODSIM
/ST_tW_antitop_5f_inclusiveDecays_TuneCP5_13TeV-powheg-pythia8/*_ext1-v1/MINIAODSIM
/ST_tW_top_5f_inclusiveDecays_TuneCP5_13TeV-powheg-pythia8/*_ext1-v1/MINIAODSIM
/ggH_HToSSTo4Tau_MH-125_TuneCP5_13TeV-powheg-pythia8/*-v1/MINIAODSIM

APPENDIX B

OTHERS

REFERENCES

[1] S.Abachi et al. "Search for High Mass Top Quark Production in pp Collisions at s = 1.8 TeV." In: *Phys. Lett.* 74 (1995), p. 12. DOI: 10.1103/PhysRevLett.74.2422. arXiv: 9411001 [hep-ex].

[2] F.Abe et al. "Observation of Top Quark Production in pp Collisions with the Collider Detector at Fermilab." In: *Phys. Lett.* 74 (1995), p. 21. DOI: 10.1103/PhysRevLett.74.2626. arXiv: 9503002 [hep-ex].

[3] Serguei Chatrchyan et al. "Observation of a New Boson at a Mass of 125 GeV with the CMS Experiment at the LHC." In: *Phys. Lett.* B716 (2012), pp. 30–61. DOI: 10.1016/j.physletb.2012.08.021. arXiv: 1207.7235 [hep-ex].

[4] Georges Aad et al. "Observation of a new particle in the search for the Standard Model Higgs boson with the ATLAS detector at the LHC." In: *Phys. Lett.* B716 (2012), pp. 1–29. DOI: 10.1016/j.physletb.2012.08.020. arXiv: 1207.7214 [hep-ex].

[5] Y.Fukuda et al. "Evidence for Oscillation of Atmospheric Neutrinos." In: *Phys. Lett.* 81 (1998), p. 9. DOI: 10.1103/PhysRevLett.81.1562. arXiv: 9807003 [hep-ex].

[6] Matthew Baumgart et al. "Non-Abelian Dark Sectors and Their Collider Signatures." In: *JHEP* 04 (2009), p. 014. DOI: 10.1088/1126-6708/2009/04/014. arXiv: 0901.0283 [hep-ph].

[7] David E. Kaplan, Markus A. Luty, and Kathryn M. Zurek. "Asymmetric Dark Matter." In: *Phys. Rev.* D79 (2009), p. 115016. DOI: 10.1103/PhysRevD.79.115016. arXiv: 0901.4117 [hep-ph].

[8] Yuk Fung Chan et al. "LHC Signatures of a Minimal Supersymmetric Hidden Valley." In: *JHEP* 05 (2012), p. 155. DOI: 10.1007/JHEP05(2012)155. arXiv: 1112.2705 [hep-ph].

[9] Keith R. Dienes and Brooks Thomas. "Dynamical Dark Matter: I. Theoretical Overview." In: *Phys. Rev.* D85 (2012), p. 083523. DOI: 10.1103/PhysRevD.85.083523. arXiv: 1106.4546 [hep-ph].

[10] Keith R. Dienes, Shufang Su, and Brooks Thomas. "Distinguishing Dynamical Dark Matter at the LHC." In: *Phys. Rev.* D86 (2012), p. 054008. DOI: 10.1103/PhysRevD.86.054008. arXiv: 1204.4183 [hep-ph].

[11] Yanou Cui and Brian Shuve. "Probing Baryogenesis with Displaced Vertices at the LHC." In: *JHEP* 02 (2015), p. 049. DOI: 10.1007/JHEP02(2015)049. arXiv: 1409.6729 [hep-ph].

[12] T Aaltonen et al. "High-precision measurement of the W boson mass with the CDF II detector." In: *Science 376 (2022) 6589, 170-176* (2022). DOI: 10.1126/science.abk1781.

[13] Satoshi Mishima and Motoi Endo. "New physics interpretation of W-boson mass anomaly."
      In: (2022), p. 21. DOI: doi.org/10.48550/arXiv.2204.05965. arXiv: 2204.05965 [hep-ph].

[14] *CMS Supersymmetry Physics Results*. Tech. rep. Geneva: CERN, 2022. URL: https://twiki.
      cern.ch/twiki/bin/view/CMSPublic/PhysicsResultsSUS.

[15] Jared Barron and David Curtin. "On the Origin of Long-Lived Particles." In: *Journal of
      High Energy Physics* 61 (2020), p. 39. DOI: doi.org/10.48550/arXiv.2007.05538. arXiv:
      2007.05538 [hep-ph].

[16] T. Aaltonen et al. "Search for heavy metastable particles decaying to jet pairs in $p\bar{p}$ collisions
      at $\sqrt{s}$ = 1.96 TeV." In: *Phys. Rev.* D85 (2012), p. 012007. DOI: 10.1103/PhysRevD.85.
      012007. arXiv: 1109.3136 [hep-ex].

[17] V. M. Abazov et al. "Search for Resonant Pair Production of long-lived particles decaying
      to b anti-b in p anti-p collisions at s**(1/2) = 1.96-TeV." In: *Phys. Rev. Lett.* 103 (2009),
      p. 071801. DOI: 10.1103/PhysRevLett.103.071801. arXiv: 0906.1787 [hep-ex].

[18] Georges Aad et al. "Search for a light Higgs boson decaying to long-lived weakly-interacting
      particles in proton-proton collisions at $\sqrt{s}$ = 7 TeV with the ATLAS detector." In: *Phys.
      Rev. Lett.* 108 (2012), p. 251801. DOI: 10.1103/PhysRevLett.108.251801. arXiv: 1203.1303
      [hep-ex].

[19] Roel Aaij et al. "Search for long-lived particles decaying to jet pairs." In: *Eur. Phys. J.* C75.4
      (2015), p. 152. DOI: 10.1140/epjc/s10052-015-3344-6. arXiv: 1412.3021 [hep-ex].

[20] Georges Aad et al. "Search for long-lived, weakly interacting particles that decay to displaced
      hadronic jets in proton-proton collisions at $\sqrt{s}$ = 8 TeV with the ATLAS detector." In: *Phys.
      Rev.* D92.1 (2015), p. 012010. DOI: 10.1103/PhysRevD.92.012010. arXiv: 1504.03634
      [hep-ex].

[21] Georges Aad et al. "Search for massive, long-lived particles using multitrack displaced vertices
      or displaced lepton pairs in pp collisions at $\sqrt{s}$ = 8 TeV with the ATLAS detector." In: *Phys.
      Rev.* D92.7 (2015), p. 072004. DOI: 10.1103/PhysRevD.92.072004. arXiv: 1504.05162
      [hep-ex].

[22] Khachatryan et al. "Search for long-lived neutral particles decaying to quark-antiquark pairs
      in proton-proton collisions at $\sqrt{s}$ = 8 TeV." In: *Phys. Rev. D* 91 (1 Jan. 2015), p. 012007. DOI:
      10.1103/PhysRevD.91.012007. URL: https://link.aps.org/doi/10.1103/PhysRevD.91.
      012007.

[23] Georges Aad et al. "Search for pair-produced long-lived neutral particles decaying in the
      ATLAS hadronic calorimeter in *pp* collisions at $\sqrt{s}$ = 8 TeV." In: *Phys. Lett.* B743 (2015),
      pp. 15–34. DOI: 10.1016/j.physletb.2015.02.015. arXiv: 1501.04020 [hep-ex].

[24]   R. Aaij et al. "Updated search for long-lived particles decaying to jet pairs." In: *Eur. Phys. J. C* 77.12 (2017), p. 812. DOI: 10.1140/epjc/s10052-017-5178-x. arXiv: 1705.07332 [hep-ex].

[25]   Roel Aaij et al. "Search for massive long-lived particles decaying semileptonically in the LHCb detector." In: *Eur. Phys. J. C* 77.4 (2017), p. 224. DOI: 10.1140/epjc/s10052-017-4744-6. arXiv: 1612.00945 [hep-ex].

[26]   Roel Aaij et al. "Search for long-lived heavy charged particles using a ring imaging Cherenkov technique at LHCb." In: *Eur. Phys. J. C* 75.12 (2015), p. 595. DOI: 10.1140/epjc/s10052-015-3809-7. arXiv: 1506.09173 [hep-ex].

[27]   Albert M Sirunyan et al. "Search for new long-lived particles at $\sqrt{s} = 13$ TeV." In: *Phys. Lett.* B780 (2018), pp. 432–454. DOI: 10.1016/j.physletb.2018.03.019. arXiv: 1711.09120 [hep-ex].

[28]   Albert M Sirunyan et al. "Search for long-lived particles with displaced vertices in multijet events in proton-proton collisions at $\sqrt{s} =$13 TeV." In: *Phys. Rev. D* 98.9 (2018), p. 092011. DOI: 10.1103/PhysRevD.98.092011. arXiv: 1808.03078 [hep-ex].

[29]   Albert M Sirunyan et al. "Search for long-lived particles decaying into displaced jets in proton-proton collisions at $\sqrt{s} = 13$ TeV." In: *Phys. Rev. D* 99.3 (2019), p. 032011. DOI: 10.1103/PhysRevD.99.032011. arXiv: 1811.07991 [hep-ex].

[30]   Albert M Sirunyan et al. "Search for long-lived particles using nonprompt jets and missing transverse momentum with proton-proton collisions at $\sqrt{s} = 13$ TeV." In: *Phys. Lett. B* 797 (2019), p. 134876. DOI: 10.1016/j.physletb.2019.134876. arXiv: 1906.06441 [hep-ex].

[31]   Albert M Sirunyan et al. "Search for new particles decaying to a jet and an emerging jet." In: *JHEP* 02 (2019), p. 179. DOI: 10.1007/JHEP02(2019)179. arXiv: 1810.10069 [hep-ex].

[32]   *Search for long-lived particles decaying into displaced jets*. Tech. rep. CMS-PAS-EXO-19-021. Geneva: CERN, 2020. URL: https://cds.cern.ch/record/2717071.

[33]   M. Aaboud et al. "Search for the Higgs boson produced in association with a vector boson and decaying into two spin-zero particles in the $H \rightarrow aa \rightarrow 4b$ channel in *pp* collisions at $\sqrt{s} = 13$ TeV with the ATLAS detector." In: *JHEP* 10 (2018), p. 031. DOI: 10.1007/JHEP10(2018)031. arXiv: 1806.07355 [hep-ex].

[34]   Morad Aaboud et al. "Search for long-lived particles in final states with displaced dimuon vertices in *pp* collisions at $\sqrt{s} = 13$ TeV with the ATLAS detector." In: *Phys. Rev. D* 99.1 (2019), p. 012001. DOI: 10.1103/PhysRevD.99.012001. arXiv: 1808.03057 [hep-ex].

[35]   Morad Aaboud et al. "Search for the Production of a Long-Lived Neutral Particle Decaying within the ATLAS Hadronic Calorimeter in Association with a *Z* Boson from *pp* Collisions at $\sqrt{s} = 13$ TeV." In: *Phys. Rev. Lett.* 122.15 (2019), p. 151801. DOI: 10.1103/PhysRevLett.122.151801. arXiv: 1811.02542 [hep-ex].

[36] Morad Aaboud et al. "Search for long-lived particles produced in pp collisions at $\sqrt{s} = 13$ TeV that decay into displaced hadronic jets in the ATLAS muon spectrometer." In: *Phys. Rev. D* 99.5 (2019), p. 052005. DOI: 10.1103/PhysRevD.99.052005. arXiv: 1811.07370 [hep-ex].

[37] Morad Aaboud et al. "Search for heavy long-lived multicharged particles in proton-proton collisions at $\sqrt{s} = 13$ TeV using the ATLAS detector." In: *Phys. Rev. D* 99.5 (2019), p. 052003. DOI: 10.1103/PhysRevD.99.052003. arXiv: 1812.03673 [hep-ex].

[38] Morad Aaboud et al. "Search for heavy charged long-lived particles in the ATLAS detector in 36.1 fb^{-1} of proton-proton collision data at $\sqrt{s} = 13$ TeV." In: *Phys. Rev. D* 99.9 (2019), p. 092007. DOI: 10.1103/PhysRevD.99.092007. arXiv: 1902.01636 [hep-ex].

[39] Morad Aaboud et al. "Search for long-lived neutral particles in pp collisions at $\sqrt{s} = 13$ TeV that decay into displaced hadronic jets in the ATLAS calorimeter." In: *Eur. Phys. J. C* 79.6 (2019), p. 481. DOI: 10.1140/epjc/s10052-019-6962-6. arXiv: 1902.03094 [hep-ex].

[40] Georges Aad et al. "Search for heavy neutral leptons in decays of W bosons produced in 13 TeV pp collisions using prompt and displaced signatures with the ATLAS detector." In: *JHEP* 10 (2019), p. 265. DOI: 10.1007/JHEP10(2019)265. arXiv: 1905.09787 [hep-ex].

[41] Georges Aad et al. "Search for Magnetic Monopoles and Stable High-Electric-Charge Objects in 13 Tev Proton-Proton Collisions with the ATLAS Detector." In: *Phys. Rev. Lett.* 124.3 (2020), p. 031802. DOI: 10.1103/PhysRevLett.124.031802. arXiv: 1905.10130 [hep-ex].

[42] Georges Aad et al. "Search for displaced vertices of oppositely charged leptons from decays of long-lived particles in pp collisions at $\sqrt{s} =13$ TeV with the ATLAS detector." In: *Phys. Lett. B* 801 (2020), p. 135114. DOI: 10.1016/j.physletb.2019.135114. arXiv: 1907.10037 [hep-ex].

[43] Georges Aad et al. "Search for long-lived neutral particles produced in pp collisions at $\sqrt{s} = 13$ TeV decaying into displaced hadronic jets in the ATLAS inner detector and muon spectrometer." In: *Phys. Rev. D* 101.5 (2020), p. 052013. DOI: 10.1103/PhysRevD.101.052013. arXiv: 1911.12575 [hep-ex].

[44] Georges Aad et al. "Search for light long-lived neutral particles produced in pp collisions at $\sqrt{s} = 13$ TeV and decaying into collimated leptons or light hadrons with the ATLAS detector." In: *Eur. Phys. J. C* 80.5 (2020), p. 450. DOI: 10.1140/epjc/s10052-020-7997-4. arXiv: 1909.01246 [hep-ex].

[45] A.Tumeysan et al. "Search for long-lived particles produced in association with a Z boson in proton-proton collisions at s = 13 TeV." In: *JHEP.* (2021), p. 36. DOI: 10.1103/PhysRevLett.74.2422. arXiv: 2110.13218 [hep-ex].

[46] Brooks Thomas Shufang Su. "The LHC Discovery Potential of a Leptophilic Higgs." In: *Phys.Rev.D79:095014,2009* (2009), p. 25. DOI: 10.1103/PhysRevD.79.095014. arXiv: 0903.0667 [hep-ph].

[47] Z. Chacko, Hock-Seng Goh, and Roni Harnik. "The Twin Higgs: Natural electroweak breaking from mirror symmetry." In: *Phys. Rev. Lett.* 96 (2006), p. 231802. DOI: 10.1103/PhysRevLett.96.231802. arXiv: hep-ph/0506256 [hep-ph].

[48] Gustavo Burdman et al. "Folded supersymmetry and the LEP paradox." In: *JHEP* 02 (2007), p. 009. DOI: 10.1088/1126-6708/2007/02/009. arXiv: hep-ph/0609152 [hep-ph].

[49] Haiying Cai, Hsin-Chia Cheng, and John Terning. "A Quirky Little Higgs Model." In: *JHEP* 05 (2009), p. 045. DOI: 10.1088/1126-6708/2009/05/045. arXiv: 0812.0843 [hep-ph].

[50] Nathaniel Craig et al. "Naturalness in the Dark at the LHC." In: *JHEP* 07 (2015), p. 105. DOI: 10.1007/JHEP07(2015)105. arXiv: 1501.05310 [hep-ph].

[51] David Curtin and Christopher B. Verhaaren. "Discovering Uncolored Naturalness in Exotic Higgs Decays." In: *JHEP* 12 (2015), p. 072. DOI: 10.1007/JHEP12(2015)072. arXiv: 1506.06141 [hep-ph].

[52] Csaba Csaki et al. "Searching for displaced Higgs boson decays." In: *Phys. Rev.* D92.7 (2015), p. 073008. DOI: 10.1103/PhysRevD.92.073008. arXiv: 1508.01522 [hep-ph].

[53] Khachatryan et al. *Muon POG – Muon Identification Run2*. 2020. URL: https://twiki.cern.ch/twiki/bin/viewauth/CMS/SWGuideMuonIdRun2.

[54] Matteo Cacciari, Gavin P. Salam, and Gregory Soyez. "The anti-k_t jet clustering algorithm." In: *JHEP* 04 (2008), p. 063. DOI: 10.1088/1126-6708/2008/04/063. arXiv: 0802.1189 [hep-ex].

[55] Khachatryan et al. *Jet Identification Run2 – 2018*. 2020. URL: https://twiki.cern.ch/twiki/bin/view/CMS/JetID13TeVRun2018.

[56] C. Mariotti Heinemeyer et al. "Handbook of LHC Higgs Cross Sections: 3. Higgs Properties." In: (2013), p. 404. DOI: 10.5170/CERN-2013-004. arXiv: 1307.1347 [hep-ph].

[57] S. Agostinelli et al. "GEANT4: A Simulation toolkit." In: *Nucl. Instrum. Meth. A* 506 (2003), pp. 250–303. DOI: 10.1016/S0168-9002(03)01368-8.

[58] Khachatryan et al. *Physics Performance Datasets – PPD Run2 Analysis Recipe Summary*. 2020. URL: https://twiki.cern.ch/twiki/bin/viewauth/CMS/PdmVAnalysisSummaryTable.

BIOGRAPHICAL SKETCH

The author was born, and then the author was "educated," at least to some degree. After finishing high school, the author completed a Bachelor of Science degree at Washington University in St.Louis. Following a decade in the work force in his discipline, the author went to FSU to pursue graduate work.